Journal of Medicinal Chemistry

Article

Synthesis and Mechanism of Hypoglycemic Activity of Benzothiazole Derivatives

Ella Meltzer-Mats, Gali Babai-Shani, Lily Pasternak, Neta Uritsky, Tamar Getter, Olga Viskind, J#rgen Eckel, Erol Cerasi, Hanoch Senderowitz, Shlomo Sasson, and Arie Gruzman

J. Med. Chem., **Just Accepted Manuscript** • DOI: 10.1021/jm4001488 • Publication Date (Web): 10 Jun 2013

Just Accepted

Journal of Medicinal Chemistry is published by the American Chemical Society. 1155 Sixteenth Street N.W., Washington, DC 20036

Synthesis and Mechanism of Hypoglycemic Activity of Benzothiazole Derivatives

Ella Meltzer-Mats[§], Gali Babai-Shani[∂], Lily Pasternak[∂], Neta Uritsky[§], Tamar Getter[§], Olga Viskind[∂,§], Jürgen Eckel[‡], Erol Cerasi[†], Hanoch Senderowitz[§], Shlomo Sasson[∂] and Arie Gruzman,[§]**

[§]Division of Medicinal Chemistry, Department of Chemistry, Faculty of Exact Sciences, Bar Ilan University, Ramat Gan, 52900, Israel

[∂]Department of Pharmacology, Institute for Drug Research, School of Pharmacy, Faculty of Medicine, The Hebrew University of Jerusalem, 91120, Jerusalem, Israel

[‡]German Diabetes Center, Integrative Physiology, Paul-Langerhans-Group, Auf'm Hennekamp 65, 40225, Düsseldorf, Germany

[†]The Endocrinology and Metabolism Service, Department of Medicine, Hadassah-Hebrew University Medical Center, Jerusalem, 91120, Israel

ABSTRACT

AMP-activated protein kinase (AMPK) has recently emerged as a major potential target for novel antidiabetic drugs. We studied the structure of 2-chloro-5-((*Z*)-((*E*)-5-((5-(4,5-dimethyl-2-nitrophenyl)furan-2-yl)methylene)-4-oxothiazolidin-2-ylidene)amino)benzoic acid (PT-1), which attenuates the autoinhibition of the enzyme, for the design and synthesis of different benzothiazoles with potential antidiabetic activity. We synthesized several structurally-related benzothiazole derivatives that increased the rate of glucose uptake in L6 myotubes in an AMPK-dependent manner. One compound, 2-(benzo[*d*]thiazol-2-ylmethylthio)-6-ethoxybenzo[*d*]thiazole (**34**), augmented the rate of glucose uptake up to 2.5-fold comparing with vehicle-treated cells and up to 1.1 fold comparing to PT-1. Concomitantly, it elevated the abundance of GLUT4 in the plasma membrane of the myotubes and activated AMPK. Subcutaneous administration of **34** to hyperglycemic Kuo Kondo rats carrying the Ay-yellow obese gene (KKAy) mice lowered blood glucose levels towards the normoglycemic range. In accord with its activity, compound **34** showed a high fit value to a pharmacophore model derived from the PT-1.

MANUSCRIPT TEXT

Introduction

A major pathophysiological defect in T2DM patients is decreased glucose utilization in peripheral tissues, such as skeletal muscles and fat depots, which aggravates hyperglycemia. [1,2] Clinical observations in diabetic patients suggest that hyperglycemia *per se* contributes and even worsens this phenomenon. [3-5] Previously, we reported that high glucose levels reduce the rate of glucose transport in skeletal muscle cells *in vivo* and *in vitro*. [5-9] This autoregulatory mechanism protects the intracellular environment against deleterious effects of an excessive glucose influx. Nonetheless, this feedback loop may also worsen the hyperglycemia and contribute further to the development of peripheral insulin resistance. Agents that increase the rate of glucose entry to skeletal muscles under hyperglycemic conditions independent of insulin are therefore invaluable for the development of novel antidiabetic drugs. [10,11]

The enzyme AMPK, which acts as a sensor of cellular energy status, plays a central role in the regulation of glucose transport in skeletal muscles. [12] Several AMPK isoenzymes have been identified, of which AMPKα2 is most abundant in skeletal muscles. [13] This enzyme is physiologically activated when the AMP:ATP ratio is increased in cells. Among other functions, activated AMPK promotes the translocation of glucose transporter 4 (GLUT4)-containing vesicles to the plasma membrane, thus increasing glucose influx in a non-insulin dependent manner. [14,15] These properties make AMPK a key target for the development of antidiabetic drugs. [16] Several classes of direct and indirect activators of AMPK such as A769662, PT-1, 5-Aminoimidazole-4-carboxamide-1-β-D-ribofuranoside (AICAR) (direct activators) and berberine, D942, momordicosides, capsaicinoids, curcumin and lipoic acid (indirect activators) have been reported. [17,18] Additionally, two large groups of antidiabetic drugs (biguanides and thiazolidinediones) owe part of their antihyperglycemic properties to the activation of AMPK. [18] Recently, the American Diabetes Association (ADA) and the European Association for the Study of Diabetes (EASD) recommended metformin (biguanide AMPK activator) as the first choice for

the monotherapy treatment of T2DM and suggested to include it in diabetes combination therapy. [19] However, side effects, such as lactic acidosis and development of tolerance to metformin emphasize the need for more potent and tissue specific AMPK activators with reduced side effects.

In this study we aimed at designing and synthesizing novel and potent activators of AMPK in skeletal muscles. The known AMPK activator PT-1, which attenuates the autoinhibition of AMPK, [20] was selected as a starting compound in our attempts to design effective AMPK activators (Chart 1). Based on medicinal chemistry principles and SAR studies of PT-1 we designed and synthesized *in house* a series of benzothiazole derivatives that were then screened for their glucose uptake increasing effects and activation of AMPK in L6 myotubes, and tested in diabetic KKAy mice in terms of amelioration of hyperglycemia. In order to unveil the molecular determinants responsible for the AMPK activation of this class of compounds and to direct future synthesis efforts we have used the data obtained in this study to develop a pharmacophore model for benzothiazole-based AMPK activators.

Results and Discussion

Pang *et al.* have reported that PT-1 (Chart 1) activated dose-dependently AMPK by relieving the autoinhibition of the enzyme. [20] In this study also showed that PT-1 increased dose- and time-dependently the phosphorylation of AMPK and its downstream substrate acetyl CoA carboxylase (ACC) in L6 myotubes, without modulating the cellular AMP:ATP ratio. We aimed at elucidating the structural moieties of PT-1 that were required to activate AMPK and increase the rate of glucose uptake in L6 myotubes. When tested in in L6 myocytes we found that PT-1 increased the rate of glucose uptake, reaching maximal effects (1.4 ±0.06-fold) at 5 μM (Supplemental Figure 1). Thus, to identify the minimal effective moiety of PT-1 required to activate AMPK and stimulate glucose uptake, several commercially available heterocyclic compounds, which were selected based on structural similarity with the (2Z,5E)-5-ethylidene-2-(methylimino)thiazolidin-4-one moiety. A substructure of PT-1: (*E*)-2-amino-5-((*E*)-3-(5-nitrofuran-2-yl)allylidene)thiazol-4(5*H*)-one (**2**) (Chart 1) at much higher concentration then PT-1 (>0.5 mmol/L) only slightly increased the rate of glucose uptake in L6

myotubes and marginally induced Thr^{172} phosphorylation in AMPK (data not shown). Of the 9 derivatives (all these compounds were randomly selected because of their structure similarity to **2**) tested only 2-amino-5-ethylthiazol-4(5*H*)-one (**3**) was active (Table 1). Figure 1 (A and B) shows that at maximal effective concentration (100 μM) **3** increased glucose uptake in L6 myotubes by 134.9% ± 11.4% (in comparison with the vehicle-treated control) within 5 h of incubation. Above this concentration **3** exhibited cytotoxic effects. The time-course analysis in Figure 1A shows that the stimulatory effect of **3** peaked at 5 h and then gradually declined to the basal level. Compound **3**-induced Thr^{172} phosphorylation in AMPK was maximal at 40 min of incubation and returned to the basal level after 3 h (Figure 1C). Other, more bulky, compounds structurally related to (2Z,5E)-5-ethylidene-2-(methylimino)thiazolidin-4-one moiety of PT-1 that include benzene moieties were purchased and tested (Table 2). Among these compounds, only compounds **4** and **15**: 6-ethoxybenzo[*d*]thiazole-2-thiol and 6-bromobenzo[*d*]thiazol-2-ol, respectively, significantly induced AMPK phosphorylation and increased the rate of glucose uptake in L6 myotubes (179.1±9.5% and 144.1%±8.8%, respectively, compared to DMSO-treated L6 myotubes; Figure 1B). The maximal effective concentration of both compounds (100 μM) was similar to that of **3**, yet, their stimulatory effect on glucose uptake persisted for 24 h (Figure 1A and 1B) and was accompanied by a stable Thr^{172} phosphorylation of AMPK during this period (Figure 1C and 1D). Compounds **3-18** lacked synergetic or additive effects to the stimulatory effect of insulin on glucose uptake in L6 myotubes (See Supplementary Table 1).

Since **4** was more effective than **15** in increasing the rate of glucose transport, it was used as a starting compound for the design and synthesis of more potent and efficacious derivatives. The first step was to investigate the role of the ethoxy moiety in **4** on its biological activity. Thus, the ethoxy moiety was removed from the corresponding phenol alcohol derivative following an overnight reaction with $AlCl_3$ in dichloroethane at room temperature, to obtain 2-mercaptobenzo[*d*]thiazol-6-ol (**19**), as described by Woltersdorf *et al.* [21] When tested in L6 myotube cultures, **19** failed to stimulate glucose

uptake, most likely due its substantial low lipophilicity (LogP=1.957±0.420) in comparison with the parent compound **4** (LogP=3.167±0.436) in resulting poor cellular membrane penetration. [22] We further synthesized three other novel compounds: 2-((2,2-diethoxyethyl)thio)benzo[*d*]thiazol-6-ol (**20**), 2-(2-ethylbutylthio)benzo[*d*]thiazol-6-ol (**21**) and 2-(butylthio)benzo[*d*]thiazol-6-ol (**22**), which were more lipophilic than **4** due to the alkylation of the free thiol group. The alkylation was performed in the presence of an excess of sodium hydride in dry THF (Scheme 1). The alkylation occurred selectively on the thiol group of **19** and did not involve the unprotected phenol moiety, likely due to lower nucleophilic property of the phenol group in comparison with the thiol moiety. Compound **20** was not stable during purification by column chromatography (*e.g.*, silica gel or alumina), as confirmed by MS analysis. Thus, it was used in cell cultures immediately after synthesis without additional purification. None of these derivatives (**20**-**22**) increased significantly the rate of glucose uptake in L6 myotubes.

Since the elimination of the ethoxy moiety from the benzene ring in **4** abolished its biological activity, regardless of the alkylation state of the free thiol group, the alkyl moiety was preserved in further syntheses. Therefore, the free thiol group was replaced by various lipophilic thioether functional groups to produce **23**-**27** (Scheme 1). In addition, the role of the carboxylic group was investigated through the synthesis of 2-(6-ethoxybenzo[*d*]thiazol-2-ylthio)acetic acid (**23**) and 3-(6-ethoxybenzo[*d*]thiazol-2-ylthio)propanoic acid (**24**). The corresponding iodo-, bromo- alkyl or 3-chloroacetic-, 3-chloropropionic acids were reacted with the thiol group of **4** in the presence of an excess of sodium hydride in dry THF. When tested in L6 myotubes only compound **24** was active. Figure 2 shows that 50 μM of **24** increased the rate of glucose uptake 1.8-fold within 5 h of incubation, in comparison with the vehicle-treated cells. Additionally, Thr^{172} phosphorylation of AMPK peaked at 60 min of incubation.

Next, we changed the thiol group in **4** to sulfonylamide or disulfane moieties, which are less prone to oxidation. [23] The former was exchanged by sulfanilamide to produce 6-ethoxybenzo[*d*]thiazole-2-sulfonamide (**28**), using a two-step synthesis according to Schoenwald *et al*. [24] Briefly, compound **4**

was treated with ammonium hydroxide (28%) and sodium hypochlorite (5.25%) in an aqueous solution and the corresponding sulfonamide derivative generated with 84% yield. The latter was oxidized with $KMnO_4$ in acetone/water (1:1) to yield **28**. This compound was inactive in the glucose uptake assay in L6 myotubes. Further, compounds 1,2-bis(6-ethoxybenzo[*d*]thiazol-2-yl)disulfane (**29**) and 1,2-di(1*H*-benzo[*d*]imidazol-2-yl)disulfane (**30**) were synthesized, as shown in Scheme 2, using a novel synthetic method, in which the corresponding thiol was refluxed overnight in the presence of concentrated HCl in THF to obtain **29**. This compound consists of two molecules of **4** covalently bound by an S-S bond. Compound **30** was similarly prepared using two 1*H*-benzoimidazole-2-thiol molecules that were coupled**.** In contrast to **29**, the sulfur atoms in both benzothiazole moieties in **30** were replaced with nitrogen atoms and the ethoxy moiety on the benzene ring was also removed. Compound **30** had a weak stimulatory effect on glucose uptake in L6 myotubes (135± 12.2%). In contrast, **29** substantially increased the rate of uptake: a maximal effect (189.0 ± 21.8%) was obtained with 150 μM within 5 h of incubation. It also induced Thr^{172} phosphorylation in AMPK within 40 min of incubation, an effect that persisted throughout the 5 h incubation (Figure 2). These effects correlate well with the increased lipophilicity and enhanced cell permeability of **29** compared with the monomeric form (**4**) that presents a free SH group. It is also suggested that the S-S bond in **29** is cleaved intracellularly to release free **4**. Nonetheless, despite its marked stimulatory effect on the glucose transport system in L6 myotubes, the potency of **29** was considered poor (maximal effective concentration above 100 μM).

To improve this low potency, benzo[*d*]thiazol derivatives were synthesized: conjugation of 6-ethoxybenzo[*d*]thiazol-2-amine or 4-(6-methylbenzo[*d*]thiazol-2-yl)aniline with 2-(chloromethyl)benzo[*d*]thiazole yielded two novel compounds: *N*-(benzo[*d*]thiazol-2-ylmethyl)-6-ethoxybenzo[*d*]thiazol-2-amine (**31**) and *N*-(benzo[*d*]thiazol-2-ylmethyl)-4-(6-methylbenzo[*d*]thiazol-2-yl)aniline (**32**), as shown in Scheme 3. Yet, both **31** and **32** were inactive in the glucose uptake assay in L6 myotubes (data not shown).

Finally, thioether derivatives of **4** were synthesized, namely, 2-(6-ethoxybenzo[*d*]thiazol-2-ylthio)-*N*-propylacetamide (**33**) and **34**, as shown in Schemes 1 and 3. Compound **33** was obtained by coupling propylamine hydrochloride with **23**, using 3-(ethyliminomethyleneamino)-*N,N*-dimethyl-propan-1-amine (EDC) with 1-hydroxybenzotriazole (HOBt) in chloroform.[25] A two-step procedure was employed in the synthesis of **34**. First, commercially available 2-methylbenzo[*d*]thiazole was transformed into 2-(chloromethyl)benzo[*d*]thiazole intermediate by chlorination (thrichloroisocyannuric acid was used for selective chlorination of the methyl group). The resulting 2-(chloromethyl)benzo[*d*]thiazole was then condensed with **4,** using a di-*iso*-propylethyl amine catalysis in dry THF. Figure 2 (A and B) shows that both compounds markedly increased the rate of glucose uptake in L6 myotubes dose- and time-dependently. The lipophilic amide derivative **33** was somewhat less potent and effective than the benzothiazol derivative **34**: 100 μM of **33** increased 2-fold the rate of glucose uptake in L6 myotubes within 5 h of incubation, compared with the 2.5-fold increase induced by **34** under similar experimental conditions. Moreover, the minimal effective concentration of **34** was 25 μM and its stimulatory effect remained unaltered up to 24 h. The time course of Thr^{172} phosphorylation of AMPK induced by **33** and **34** varied: the former induced significant Thr^{172} phosphorylation after 3 h of incubation while the latter caused it already within 1 hour (Figure 2C and 2D).

Compound **34** was the most promising benzothiazole derivative, and its biological activity was further studied. The compound also has drugable LogP (4.34±0.14) and water solubility (12.09 ±1.71 μM/L); both parameters were experimentally determined as described in the Supplemental Information, D1. Figure 2E shows that **34** increased dose-dependently Thr^{172} phosphorylation in AMPK in L6 myotubes: already at 5 μM **34** noticeably induced phosphorylation, while at 150 μM it raised it 7.6 fold in comparison with DMSO-treated control myotubes. Figure 3A shows additivity in glucose transport stimulatory effects of **34** and insulin in L6 myotubes, suggesting distinct and independent mechanisms of actions of **34** and insulin.

Further, AMPK-induced phosphorylation of ACC and AMPK substrate 160 kDa (AS-160) was determined. Figure 3B shows that **34** significantly induced Ser^{79} and Thr^{642} phosphorylation of ACC and AS-160, respectively. The classical AMPK activators: AICAR (4 mmol/L) and D-sorbitol (hyperosmolar shock inducer at 0.25 M) served as positive controls in this experiment. Additionally, Compound C, a selective inhibitor of AMPK [26] was used to analyze the role of AMPK in mediating the action of **34**. When added (5 μM) to myotube cultures, it significantly impeded the ability of **34** to augment the phosphorylation of both AMPK substrates in L6 myotubes. The activation of ACC leads to increased production of malonyl-CoA, [27] which further inhibits carnitine acyl-CoA transferase-1, the enzyme that transports fatty acids into mitochondria and leads to the inhibition of mitochondrial fatty acid degradation. [28] To exclude the possibility that the activation of ACC inhibited fatty acid metabolism and caused cytotoxicity, we assessed potential cytotoxic effects of **34** in the (3-(4,5-Dimethylthiazol-2-yl)-2,5-diphenyltetrazolium bromide test (MTT). This assay measures the reduction of a tetrazolium salt into a formazan product by dehydrogenase enzymes in functional mitochondria. [29] The data in Supplemental Figure 2 show that L6 myotube viability remained intact upon exposure to high concentrations of **34** during prolonged incubation periods. Thapsigargin-induced apoptosis served as a positive control in this assay. [30] Reduced cellular ATP levels and increased ATP:AMP ratio are associated with upregulation of glucose transport and AMPK activation, respectively. [31,32] Therefore, we tested whether **34** induced such effects; Table 3 shows that the cellular concentration of ATP was unaltered in the presence of 200 μM **34** in myotube cultures. Thus, it appears that the stimulatory effect of **34** on AMPK was unrelated to cellular AMP level.

The ability of compound **34** to mobilize GLUT4-rich vesicles to the plasma membrane of myotubes was then investigated using the myc-tagged-GLUT4 L6 or myc-tagged-GLUT1 L6 cell lines. In this assay the abundance of the myc epitope embedded in the first extracellular loop of the transporter is determined by a colorimetric immunodetection assay. [33] Figure 3C shows that insulin and **34** independently increased the abundance of GLUT4myc, but not GLUT1myc, in the plasma membrane of

L6 myotubes. The effect of insulin on the GLUT4myc translocation to the plasma membrane of myotubes was fast (30 min) whereas **34** exerted its effects following a 5-h incubation period. Neither agent altered the total content of GLUT4 or GLUT1 in myotubes, as determined in whole cell lysates of treated L6 myotubes (insert, Figure 3C).

The fact that **34** increased GLUT4 content in the plasma membrane raised the possibility that **34** could employ the insulin transduction pathway to mobilize GLUT4-containing vesicles to the plasma membrane. To this end, the phosphatidylinositide 3-kinase (PI3K) inhibitor wortmannin and an Akt/PKB inhibitor (1,3-Dihydro-1-(1-((4-(6-phenyl-1*H*-imidazo[4,5-*g*]quinoxalin-7-yl)phenyl)methyl)-4-piperidinyl)-2*H*-benzimidazol-2-one tri-fluoroacetate salt hydrate) were used in **34**-treated cells. [34] In control myotubes, both inhibitors suppressed insulin-stimulated glucose uptake; however, the stimulatory effect of **34** on glucose uptake remained intact in the presence of each inhibitors (Figure 3D), suggesting that the insulin transduction mechanism was not involved in mediating **34**-induced recruitment of GLUT4 to the surface of L6 myotubes. Conversely, the AMPK inhibitor compound C completely blocked **34**-mediated stimulation of the rate of glucose transport in L6 myotubes. Additionally, we used a commercial available kit to determine the AMPK activity in vitro, as described in Figure 3E. In this assay PT-1 or **34** markedly increased the kinase activity of recombinant human full length AMPK by 2.04.0±0.04 and 4.30±0.05-fold, respectively, comparing with the DMSO treated control. These findings suggest that **34** also interacts with AMPK and modifies it catalytic activity.

KKAy mice develop diabetic traits similar to those characterizing T2DM patients, including hyperinsulinemia, hyperglycemia, obesity, and peripheral resistance to insulin, and several studies indicate they are an excellent animal model for *in vivo* evaluation of antidiabetic drugs. [35] Therefore, we tested the antihyperglycemic potential of **34** by subcutaneously injecting it to diabetic KKAy mice (30 or 75 mg/kg body weight, suspension in sesame oil, twice daily), while the control group received the vehicle only. Oral (gavage) administration of **34** to these mice failed to lower significantly blood glucose levels, possibly due to a low biostability of **34** (Supplemental Information, D2). Indeed when

incubated with mouse hepatic microsomes **34** was subjected to a rapid Phase I metabolism with an *in vitro* estimated half-life time of 2.4 min and rapid clearance (692 μl/min/mg). In addition, **34** significantly inhibited CytP450 2D6 and 3A4 activity by 64.4% ±4.9% and 77.1% ±11.5%, respectively, an in vitro assay (Supplemental Information D3). The activity of 1A2, 2C9 and 2C19 isoforms of P450 was not affected in the presence of **34**. Figure 4A shows a substantial blood glucose lowering effect of **34**: it reduced blood glucose by nearly 30%, 45% and 50% on days 1, 2 and 3 of treatment, respectively, whereas the oil treatment (vehicle) had no effect. It should also be noted that despite the marked antihyperglycemic effects of **34**, normoglycemia was not attained. In addition, food intake of **34**-treated mice was not significantly different from the that measured in the cages of control mice. Furthermore, ip-GTT was performed in KKAy mice treated with **34** for two days after an overnight fast, as described. [6] Figure 4B shows improved tolerance to glucose in comparison with the vehicle-treated group. In the treated mice the AUC were 1523.9 ± 132.9 vs. 1150.6 ± 125.8 or 753.6 ± 142.2 mmol glucose/l/min for oil-treated and 30 or 75 mg/kg **34**-treated KKAy mice, respectively. The daily food intake was not affected by **34**, as shown in Supplemental Table 6. These results show that **34** improved total body glucose clearance in diabetic KKAy mice by 40%-50% following a two-day treatment.

While the design strategy of the compounds synthesized and tested in this work was based on medicinal chemistry considerations, we have performed a post-synthesis pharmacophore analysis of the results with three main goals in mind: (1) Rationalize the design strategy and experimental (tested compounds activity) data (2) Elucidate the structural determinant responsible for the biological activity; (3) Direct future synthesis efforts. With this in mind, we have first generated a 3D pharmacophore model from the lowest energy conformation of the starting compound (PT-1). The resulting pharmacophore (Figure 5A) consists of two aromatic moieties corresponding to the furan ring and the 5-amino-chloro benzoic acid ring, three hydrophobic centers located on the chlorine atom of the 5-amino-chloro benzoic acid ring and on the benzene moiety and the methyl group of the terminal 1,2-dimethyl-

4-nitrobenzene ring and four H-bond acceptors located on the carboxylic group, the sulfur atom of the central thiazolidine ring, the carbonyl oxygen of the same ring and on the nitro moiety of the 1,2-dimethyl-4-nitrobenzene ring. The fit of PT-1 to this model is, not surprisingly, good (fit value of 9; see Figure 5A and Supplemental Table 4). Next, we have screened compounds **2**-**4** (Chart 1) against this model and in accord with the biological results (Table 2), and found compound **4** to have the best fit values among the three. Moreover, this compound fits almost equally well into two, largely non-overlapping parts of the pharmacophore model (fit values of 2.49 and 2.23, Figure 5B), thereby justifying the overall design strategy, which was largely based on tethering together two analogs of this compound. Finally, all 31 compounds tested in this work were screened into the pharmacophore model. The results are presented in Supplemental Table 4 and confirm that, overall; the more active compounds have better fit values. Using a cutoff of 3, 5 out of 6 active compounds (83% success) have a fit value above this number whereas 22 out of 25 inactive compounds (88% success) have fit values below it or do not map to the pharmacophore model at all. In particular our lead compound (**34)**, fits into the pharmacophore model with a fit value of 4.63 (Figure 5C).

While our preliminary pharmacophore model gave reasonable results, it was developed from a single compound and consequently does not take advantage of the new data obtained in this work. With this in mind, we have developed a new pharmacophore model based on the three most active compounds (**29**, **33**, **34**) and further refined it based on data on 2 inactive compounds (**25** and **31**, see method section for more details). The resulting pharmacophore (Figure 6A) consists of a single aromatic moiety located on the central phenyl ring, five hydrogen bond acceptors located on the sulfur and on the nitrogen atoms of the benzothiazole group, on the sulfur atom of the linker between the two benzothiazole rings, on the oxygen of the ethoxy group that is connected to the benzothiazole moiety and on the second ("right hand side") benzothiazole moiety and two hydrophobic moieties located on the ethoxy group and on the phenyl group of the second benzothiazole moiety. The fit values resulting from the mapping of the compounds considered in this work into this pharmacophore model are

presented in Supplemental Table 5 and show that all of the active compounds are characterized by high fit values (above cutoff of 19; 100% success) whereas 24 out of the 25 inactive compounds are characterized by values below this threshold (96% success). In particular, this pharmacophore model well explained the activity difference between **34** (active) and its close, albeit inactive analog **31**. These two compounds differ by a single moiety, namely, a sulfur atom in **34** that maps into an H-bond acceptor pharmacophoric feature versus an NH group (an H-bond donor) in **31** (see arrows in Figure 6B-C).

While the two pharmacophores were built based on different structures they share many common features, in particular in the region corresponding to the ethoxybenzothiazole moiety of compound **34** (see Figures 5 and 6 where the pharmacophoric features corresponding to the ethoxybenzothiazole moiety are circled). Yet the two pharmacophores differ in the regions corresponding to the second ("right hand side") benzothiazole moiety and the linker between the two ring systems of **34**. Importantly, the H-bond acceptor feature responsible for reproducing the activity differences between compounds **34** and **31** (see above) is missing in the first pharmacophore. Accordingly, the second-generation pharmacophore outperforms the first one in terms of its ability to differentiate between active and inactive compounds (see above and Tables 4 and 5). This is not surprising since this pharmacophore was built on a larger collection of compounds taking into account both active and inactive ones. This new pharmacophore model will direct our future synthesis efforts aimed at developing yet more potent benzothiazole-based AMPK activators.

Validation of our in vitro results, that PT-1 and **34** directly activate AMPK, was conducted using the binding mode suggested by Pang. [20] Our docking simulations identified favorable interactions between PT1 and specific binding site residues. The lead compound of this study, **34** together with the reference compound PT1 were docked into the binding site of AMPK to gain additional insight into their potential interactions with the kinase. In particular, PT1 forms a salt bridge with K154 which was shown by mutation studies to be important for the binding of this compounds .[20] Additional interactions are formed with S97 and A149 (H-bonds), K78 (π-cation interaction) and P74 (π-π interaction; see

Figure 7A). Only one of these interactions is preserved for analogue 34 (H-bond with K154). However, this compound is stabilized by an additional H-bond with K41 (figure 7B). These differences in the interactions pattern between the three compounds are reflected in their overall docking scores (-5.24, -3.65 for PT1 and **34**, respectively). Overall, our docking simulations suggest that PT1 is the best binder followed by analogue **34**. However, these results do not indicate the degree to which these compounds could activate the protein.

Conclusion

Various substituted benzothiazol derivatives were synthesized and screened for their potential hypoglycemic (antihyperglycemic) activity. The ethoxybenzothiazole moiety in **34** was found to be critical for increasing glucose transport in L6 myotubes and for the activation of AMPK. In accord with this observation, this moiety fits three of the pharmacophoric features found to be important for the biologic activity (hydrophobic, aromatic and H-bond acceptor, located on the ethoxy, phenyl and thiazolidin ring, respectively; see Figure 6B). Compound **34** significantly increases the rate of glucose uptake in L6 myotubes at pharmacologically relevant concentrations (25 μM). Moreover, already at concentration of 5 μM it increased phosphorylation of AMPK in L6 myotubes.

The activity of **34** is not mediated by the insulin transduction pathway, since the inhibition of both key insulin sensitive enzymes PI3K and AKT/PKB did not alter **34**-induced stimulation of glucose uptake. The protein AS-160, shared by the insulin- and AMPK-induced GLUT4 translocation mechanisms, was markedly phosphorylated by **34**. These results emphasize an important property of **34**, namely, increasing glucose uptake in a skeletal muscle *in vitro* model (L6 myotubes) in the absence of insulin. The stimulatory effect of **34** was blocked by an AMPK inhibitor (compound C), pointing to the essential role of AMPK activation in the biological effect of **34**. The enzyme ACC, which is also activated by AMPK, is not directly related to glucose uptake regulation in skeletal muscles. However, this downstream target of AMPK was phosphorylated and activated by **34** in L6 myotubes, thereby

supporting our main conclusion that compound **34** leads to physiological phosphorylation of AMPK and activation of all its downstream pathways. Our docking simulations and direct effect of **34** on recombinant human AMPK suggest that such activation may result from a direct binding of compound **34** to AMPK. The biological relevance of these *in vitro* findings have been demonstrated by the effect of compound **34** in decreasing the blood glucose level in diabetic KKAy mice. Metabolic instability of the **34** can be improved by replacing of methyl-thio linker by more metabolic stable linkers. Thus, also may lead to oral activity of those new **34** derivatives.

Experimental Section

Materials and Methods

ATP Assay Kit (Colorimetric) and rabbit polyclonal anti-glucose transporter GLUT1 and GLUT4 antibodies were obtained from Abcam (Cambridge, MA). Human insulin (Actrapid) was purchased from Novo Nordisk (Bagsvaerd, Denmark). AICAR, BSA, MT, compound **4**, compound C, 2-deoxy-D-glucose (dGlc), D-glucose, O-phenylenediamine (OPD), and the protease inhibitor cocktail were purchased from Sigma-Aldrich Chemicals (Rehovot, Israel). Compound **2** was from Synthon-Lab Ltd. (St. Petersburg, Russia). Chemical Block Ltd. (Moscow, Russia) supplied compound **3**. Glycerol and sodium fluoride were from Merck (Whitehouse Station, NJ). Mercaptoethanol, phenylmethanesulfonylfluoride (PMSF), sodium orthovanadate, sodium-β-glycerophosphate, sodium pyrophosphate and SDS were purchased from Alfa Aesar (Ward Hill, MA). PT-1 was supplied by Tocris (Bristol, UK). ADP-Glo^{tm} AMPK A1/B1/G1 kinase kit was purchased from SignalChem (Richmond, Canada). American Radiolabeled Chemicals (St. Louis, MO) supplied [^{3}H]dGlc [2.22 TBq/mmol (60 Ci/mmol)]. Antibodies against AMPKα, AS-160, pThr^{642}-AS-160 and pThr^{172}-AMPK were purchased from Cell Signaling Technology (Beverly, MD). ACC, pSer^{79}-ACC and α-tubuline were from Millipore (Billerica, MA). The Anti-c-Myc (A-14) antibody was from Santa Cruz Biotechnology (Santa Cruz, CA), horseradish peroxidase (HRP)-conjugated anti-rabbit IgG and EZ-ECL chemoluminescence detection kit were from Jackson ImmunoResearch (West Grove, PA). Goat serum,

fetal calf serum (FCS), L-glutamine, α-minimal essential medium (MEM) and antibiotics were purchased from Biological Industries (Beth-Haemek, Israel). Organic solvents (HPLC grade) were from Frutarom Ltd. (Haifa, Israel). Dry THF was obtained using distillation from a boiled blue color mix with sodium/benzophenone. The melting points were determined with Fisher-Johns melting point apparatus (Palmerton, PA). The ^{1}H NMR and ^{13}C NMR spectra were recorded at room temperature on a Bruker Advance NMR spectrometer (Vernon Hills, IL) operating at 200 and 300 MHz and were in accord with the assigned structures. Chemical shift values were reported relative to TMS that was used as an internal standard. The samples were prepared by dissolving the synthesized compounds in DMSO-d_6 (δ_H = 2.50 ppm, δ_C = 39.52 ppm) or in $CDCl_3$ (δ_H = 7.26 ppm, δ_C = 77.16 ppm). [36] Chemical shifts were expressed in δ (ppm) and coupling constants (*J*) in hertz. The splitting pattern abbreviations are as follows: s, singlet; d, doublet; t, triplet; q, quartet; quint, quintet; m, unresolved multiplet due to the field strength of the instrument; dd, doublet of doublet. A QTof micro spectrometer (Micromass, Milford, MA) in the positive ion mode was used for mass spectrometry. Data were processed using massLynX v.4.1 calculation and deconvolution software (Waters Corporation, Milford, MA). Column chromatography was performed on Merck Silica gel 60 (230-400 mesh; Merck, Darmstadt, Germany). Analytical and preparative HPLC (Young Lin Instruments, Anyang, Korea) were performed on LUNA C18(2) preparative (10 μm, 100 x 30 mm) or analytical (5 μm, 250 x 4.6 mm) columns, both from Phenomenex Inc. (Torrance, CA). Acetonitrile and doubly distilled water were used as an eluent in different ratios. Analytical thin layer chromatography was carried out on pre-coated Merck Silica gel $60F_{254}$ (Merck) sheets using UV absorption and iodine physical adsorption for visualization. The ≥95% purity of the final compounds **19**, **22-34** and the <95% purity of the final compounds **20**, **21** was confirmed using HPLC analysis.

General procedure for the synthesis of S-alkyl benzothiazoles (**20-22**).

To an ice-cold stirred solution of **19** (0.20 g, 1.09 mmol) in dry THF (15 mL) sodium hydride (0.11 g, 4.58 mmol) was added in three portions. Then, the appropriate alkylhalide (2.73 mmol in dry THF, 2

mL) was added drop-wise to the reaction solution. Stirring at 0 °C was continued for 1 hour followed by additional 1 hour incubation at room temperature. The reaction progress was followed by TLC (100% CH_2Cl_2). The reaction was quenched by the addition of ice (about 15 g) followed by 100 mL of chloroform. The organic layer was separated, washed twice in water, dried over sodium sulfate, filtered and evaporated to yield the solid product. The compounds were purified by column chromatography using 100% dichloromethane as an eluent.

2-(2,2-dimethoxyethylthio)benzo[d]thiazol-6-ol (**20**). Yield ~70% colorless syrup. The purity of the compound was 60% we did not succeed purifying **20** (See supplemental information). ^{1}H NMR ($CDCl_3$, 200 MHz): δ 1.43 (s, 6H, -$SCH_2CH(OC\underline{H}_3)_2$), 3.53 (d, 2H, *J*=5.4, -$SC\underline{H}_2CH(OCH_3)_2$), 4.71 (t, 1H, *J*=5.4 Hz, -$SCH_2C\underline{H}(OCH_3)_2$), 6.90-6.98 (m, 2H, HO-<u>Ph</u>-), 7.20 (d, 1H, *J*=2.4 Hz, HO-<u>Ph</u>-), 7.68 (d, 1H, *J*=9.0 Hz, HO-<u>Ph</u>-). ^{13}C NMR was not conducted because the compound disintegrated during the night NMR testing. HPLC (gradient water/CH_3CN from 100 % of water in 60 min, flow = 1 mL/min, λ = 254 nm): t_R = 40.6 min.

2-(2-ethylbutylthio)benzo[d]thiazol-6-ol (**21**). Yield 50% white powder, mp 105-110 °C. The purity of the compound was 86% we did not succeed purifying **21** more than that (See supplemental information). ^{1}H NMR ($CDCl_3$, 300 MHz): δ 0.90 (t, 6H, *J*=9.0 Hz, -$SCH_2CH(CH_2C\underline{H}_3)_2$), 1.44-1.52 (m, 4H, -$SCH_2CH(C\underline{H}_2CH_3)_2$), 1.65-1.70 (m, 1H, -$SCH_2C\underline{H}(CH_2CH_3)_2$), 3.32 (d, 2H, *J*=6.3 Hz, -$SC\underline{H}_2CH(CH_2CH_3)_2$), 6.92 (dd, 1H, *J*=2.5, 6.3 Hz, HO-<u>Ph</u>-), 7.20 (d, 1H, *J*=2.4 Hz, HO-<u>Ph</u>-), 7.71 (d, 1H, *J*=8.7 Hz, HO-<u>Ph</u>-). ^{13}C NMR ($CDCl_3$, 50 MHz): δ 10.7 (-$SCH_2CH(CH_2\underline{C}H_3)_2$), 25.1 (-$SCH_2CH(\underline{C}H_2CH_3)_2$), 37.6 (-$S\underline{C}H_2CH(CH_2CH_3)_2$), 40.5 (-$SCH_2\underline{C}H(CH_2CH_3)_2$), 106.5 (HO-<u>Ph</u>-), 115.0 (HO-<u>Ph</u>-), 121.8 (HO-<u>Ph</u>-), 129.7 (HO-<u>Ph</u>-), 141.0 (HO-<u>Ph</u>-), 143.1 (HO-<u>Ph</u>-), 154.6 (HO-Ph-<u>[*d*]thiazole</u>-S-). MS (ES^+): 267 (MH^+). HRMS (CI^+) 267.0770 (M^+), 268.076 (MH^+). HPLC (gradient water/CH_3CN from 100 % of water in 60 min, flow = 1 mL/min, λ = 254 nm): t_R = 48.2 min.

2-(butylthio)benzo[d]thiazol-6-ol (**22**). Yield 60% light brown crystals, mp 80-85 °C. ^{1}H NMR ($CDCl_3$, 300 MHz): δ 0.90 (t, 3H, *J*=7.3 Hz, -$SCH_2CH_2CH_2C\underline{H}_3$), 1.43-1.55 (m, 2H, -$SCH_2CH_2C\underline{H}_2CH_3$), 1.73-1.83 (m, 2H, -$SCH_2C\underline{H}_2CH_2CH_3$), 3.30 (t, 2H, *J*=7.3 Hz, -$SC\underline{H}_2CH_2CH_2CH_3$), 6.92 (dd, 1H, *J*=2.5, 6.3 Hz, HO-Ph-), 7.21 (d, 1H, *J*=2.4 Hz, HO-Ph-), 7.71 (d, 1H, *J*=8.7 Hz, HO-Ph-). ^{13}C NMR ($CDCl_3$, 50 MHz): δ 13.4 (-$SCH_2CH_2CH_2\underline{C}H_3$), 21.7 (-$SCH_2CH_2\underline{C}H_2CH_3$), 31.1 (-$SCH_2\underline{C}H_2CH_2CH_3$), 33.7 (-$S\underline{C}H_2CH_2CH_2CH_3$), 106.7 (HO-Ph-), 115.6 (HO-Ph-), 121.6 (HO-Ph-), 136.1 (HO-Ph-), 147.0 (HO-Ph-), 153.8 (HO-Ph-), 165.0 (HO-Ph-[*d*]thiazole-S-). MS (ES^+): 240 (MH^+). HRMS (CI^+) 239.0462 (M^+), 240.050 (MH^+). HPLC (gradient water/CH_3CN from 100 % of water in 60 min, flow = 1 mL/min, λ = 254 nm): t_R = 41.7 min.

General procedure for the synthesis of S-alkyl 6-ethoxybenzo[d]thiazoles (**25-27**).

These compounds were synthesized according to the synthetic procedure for S-alkyl benzo[*d*]thiazoles, using was **4** as the starting molecule. [37]

6-ethoxy-2-(propylthio)benzo[d]thiazole (**25**). The remaining yellow syrup was further purified by silica gel column chromatography (eluent: 100% dichloromethane). Attempts to crystallize the syrup were unsuccessful. Yield 10% colorless syrup. ^{1}H NMR ($CDCl_3$, 200 MHz): δ 1.05 (t, 3H, *J*=7.4 Hz, -$SCH_2CH_2C\underline{H}_3$), 1.41 (t, 3H, *J*=7.0 Hz, -Ph-$OCH_2C\underline{H}_3$), 1.82 (m, 2H, -$SCH_2C\underline{H}_2CH_3$), 3.26 (t, 2H, *J*=7.2 Hz, -$SC\underline{H}_2CH_2CH_3$), 4.01 (q, 2H, *J*=6.9 Hz, -Ph-$OC\underline{H}_2CH_3$), 6.97 (dd, 1H, *J*=2.5, 6.4 Hz, EtO-Ph-), 7.18 (d, 1H, *J*=2.2 Hz, EtO-Ph-), 7.73 (d, 1H, *J*=9.0 Hz, EtO-Ph-). ^{13}C NMR ($CDCl_3$, 50 MHz): δ 13.2 (-$SCH_2CH_2\underline{C}H_3$), 14.7 (-Ph-$OCH_2\underline{C}H_3$), 22.6 (-$SCH_2\underline{C}H_2CH_3$), 35.5 (-$S\underline{C}H_2CH_2CH_3$), 63.9 (-Ph-$O\underline{C}H_2CH_3$), 104.6 (EtO-Ph-), 115.0 (EtO-Ph-), 121.7 (EtO-Ph-), 136.3 (EtO-Ph-), 147.7 (EtO-Ph-), 156.2 (EtO-Ph-), 163.8 (EtO-Ph-[*d*]thiazole-S-). MS (ES^+): 254 (MH^+). HRMS (CI^+) 253.0583 (M^+), 254.064 (MH^+). HPLC (gradient water/CH_3CN from 100 % of water in 60 min, flow = 1 mL/min, λ = 254 nm): t_R = 52.1 min.

6-ethoxy-2-(2-ethylbutylthio)benzo[d]thiazole (**26**). The compound was obtained as a yellow syrup that was further purified by silica gel column chromatography (eluent: 100% dichloromethane). Attempts to crystallize the syrup were unsuccessful. Yield 10% colorless syrup. ^{1}H NMR ($CDCl_3$, 300 MHz): δ 0.93 (t, 6H, *J*=7.4 Hz, -$SCH_2CH(CH_2CH_3)_2$), 1.41-1.50 (m, 4H, -$SCH_2CH(CH_2CH_3)_2$), 1.63-1.70 (m, 1H, -$SCH_2CH(CH_2CH_3)_2$), 3.33 (d, 2H, *J*=6.3 Hz, -$SCH_2CH(CH_2CH_3)_2$), 4.05 (q, 2H, *J*=7.0 Hz, -Ph-OCH_2CH_3), 6.98 (dd, 1H, *J*=2.4, 6.6 Hz, EtO-Ph-), 7.20 (d, 1H, *J*=2.4 Hz, EtO-Ph-), 7.73 (d, 1H, *J*=9.0 Hz, EtO-Ph-). ^{13}C NMR ($CDCl_3$, 75 MHz): δ 10.9 (-$SCH_2CH(CH_2CH_3)_2$), 14.8 (-Ph-OCH_2CH_3), 25.2 (-$SCH_2CH(CH_2CH_3)_2$), 37.6 (-$SCH_2CH(CH_2CH_3)_2$), 40.7 (-$SCH_2CH(CH_2CH_3)_2$), 64.1 (-Ph-OCH_2CH_3), 104.8 (EtO-Ph-), 115.1 (EtO-Ph-), 121.8 (EtO-Ph-), 136.4 (EtO-Ph-), 147.8 (EtO-Ph-), 156.3 (EtO-Ph-[*d*]thiazole-S-). MS (ES^+): 296 (MH^+), 318 (MNa^+). HRMS (CI^+) 295.1020 (M^+), 296.106 (MH^+). HPLC (gradient water/CH_3CN from 100 % of water in 60 min, flow = 1 mL/min, λ = 254 nm): t_R = 61.1 min.

2-(butylthio)-6-ethoxybenzo[d]thiazole (**27**). The compound was purified by silica gel column chromatography (eluent: 100% dichloromethane). Yield 30% colorless crystalline needles, mp 30-35 °C. ^{1}H NMR ($CDCl_3$, 200 MHz): δ 1.12 (t, 3H, *J*=7.0 Hz, -$SCH_2CH_2CH_2CH_3$), 1.56-1.74 (m, 5H, -$SCH_2CH_2CH_2CH_3$, -Ph-OCH_2CH_3), 1.87-2.02 (m, 2H, -$SCH_2CH_2CH_2CH_3$), 3.46 (t, 2H, *J*=7.3 Hz, -$SCH_2CH_2CH_2CH_3$), 4.21 (q, 2H, *J*=7.0 Hz, -Ph-OCH_2CH_3), 7.15 (dd, 1H, *J*=2.4, 6.6 Hz, EtO-Ph-), 7.37 (d, 1H, *J*=2.6 Hz, EtO-Ph-), 7.90 (d, 1H, *J*=9.0 Hz, EtO-Ph-). ^{13}C NMR ($CDCl_3$, 50 MHz): δ 13.4(-$SCH_2CH_2CH_2CH_3$), 14.7 (-Ph-OCH_2CH_3), 21.8 (-$SCH_2CH_2CH_2CH_3$), 31.2 (-$SCH_2CH_2CH_2CH_3$), 33.4 (-$SCH_2CH_2CH_2CH_3$), 64.0 (-Ph-OCH_2CH_3), 104.7 (EtO-Ph-), 115.0 (EtO-Ph-), 121.8 (EtO-Ph-), 136.2 (EtO-Ph-), 156.1 (EtO-Ph-), 163.9 (EtO-Ph-[*d*]thiazole-S-). MS (ES^+): 268 (MH^+), 318 (MNa^+). HRMS (MALDI) 268.082 (MH^+). HPLC (gradient water/CH_3CN from 100 % of water in 60 min, flow = 1 mL/min, λ = 254 nm): t_R = 44.8 min.

General procedure for the synthesis of (6-ethoxybenzo[d]thiazol-2-yl)methanamine derivatives (**31**-**32**). To a stirred solution of commercially available 6-ethoxybenzo[*d*]thiazol-2-amine (1.00 g, 4.16 mmol) or

2-(4-aminophenyl)-6-methylbenzo[*d*]thiazole (1.00 g, 5.15 mmol) with triethylamine (1.08 mL, 7.72 mmol or 0.87 mL, 6.24 mmol, respectively) and 4-dimethylaminopyridine (0.06 g, 0.49 mmol or 0.05 g, 0.41 mmol, respectively) in THF (35 or 50 mL, respectively) was added previously synthesized 2-(chloromethyl)benzo[*d*]thiazole according to Russell *et al*. [38] (0.94 g, 5.15 mmol or 0.76 g, 4.14 mmol). The reaction mixture stirred in room temperature or refluxed overnight, respectively. Then, the solution was cooled to room temperature, and water (100 mL) followed by chloroform (100 mL) were added. The organic layer was separated, washed twice in water, dried over sodium sulfate, filtered and evaporated. The crude solid was purified by HPLC.

N-(benzo[d]thiazol-2-ylmethyl)-6-ethoxybenzo[d]thiazol-2-amine (**31**). Yield 20% brown solid, mp 150-156 °C. ^{1}H NMR (DMSO-d_6, 200 MHz): δ 1.33 (t, 3H, *J*=6.9 Hz, -Ph-OCH$_2$C<u>H</u>$_3$), 4.04 (q, 2H, *J*=6.9 Hz, -Ph-OC<u>H</u>$_2$CH$_3$), 5.22 (s, 2H, -NH-C<u>H</u>$_2$-Ph-), 7.03 (d, 2H, *J*=8.8 Hz, EtO-<u>Ph</u>-), 7.22 (d, 2H, *J*=8.6 Hz, EtO-<u>Ph</u>-), 7.53 (m, 2H, EtO-<u>Ph</u>-), 8.09 (dd, 1H, *J*=9.0 Hz, EtO-<u>Ph</u>-). ^{13}C NMR (DMSO-d_6, 50 MHz): δ 14.6 (-Ph-OCH$_2$<u>C</u>H$_3$), 32.6 (-NH-<u>C</u>H$_2$-Ph-), 63.7 (-Ph-O<u>C</u>H$_2$CH$_3$), 115.1 (-<u>Ph</u>-OEt), 121.8 (-<u>Ph</u>-OEt), 123.1 (-<u>benzo</u>[*d*]thiazole), 126.4 (-<u>benzo</u>[*d*]thiazole), 126.6 (-<u>Ph</u>-OEt), 127.1 (-<u>benzo</u>[*d*]thiazole), 128.0 (-SCH$_2$-<u>benzo</u>[*d*]thiazole), 151.8 (-<u>Ph</u>-OEt, -<u>benzo</u>[*d*]thiazole), 159.3 (-<u>Ph</u>-OEt, -<u>benzo</u>[*d*]thiazole), 172.0 (-benzo[*d*]<u>thiazole</u>). MS (ES$^+$): 342 (MH$^+$). HPLC (gradient water/CH$_3$CN from 100 % of water in 60 min, flow = 1 mL/min, λ = 254 nm): t_R = 26.8 min.

N-(benzo[d]thiazol-2-ylmethyl)-4-(6-methylbenzo[d]thiazol-2-yl)aniline (**32**). Yield 40% yellow solid, mp 143-145 °C. ^{1}H NMR (CDCl$_3$, 400 MHz): δ 2.46 (s, 3H, C<u>H</u>$_3$-Ph-), 4.85 (s, 2H, -NH-C<u>H</u>$_2$-), 6.77 (dd, 2H, *J*=2.0, 4.8 Hz, -<u>Ph</u>-NH-), 7.24 (dd, 1H, *J*=1.4, 7.2 Hz, CH$_3$-<u>benzo</u>[*d*]thiazole), 7.38 (t, 1H, *J*=7.6 Hz, -CH$_2$-<u>benzo</u>[*d*]thiazole), 7.49 (t, 1H, *J*=7.6 Hz, -CH$_2$-<u>benzo</u>[*d*]thiazole), 7.62 (s, 1H, CH$_3$-<u>benzo</u>[*d*]thiazole), 7.83-7.91 (m, 4H, CH$_3$-<u>benzo</u>[*d*]thiazole, -CH$_2$-<u>benzo</u>[*d*]thiazole), 8.01 (d,1H, *J*=8.4 Hz, CH$_3$-<u>benzo</u>[*d*]thiazole). ^{13}C NMR (CDCl$_3$, 150 MHz): δ 21.5 (<u>C</u>H$_3$-Ph-), 46.6 (-NH-<u>C</u>H$_2$-), 113.1 (-<u>Ph</u>-NH-), 121.2 (-<u>Ph</u>-NH-), 121.8 (CH$_3$-<u>Ph</u>-), 122.0 (CH$_3$-<u>Ph</u>-), 122.9 (-<u>benzo</u>[*d*]thiazole), 124.4 (-CH$_2$-<u>benzo</u>[*d*]thiazole), 125.2 (-<u>benzo</u>[*d*]thiazole), 126.2 (-<u>benzo</u>[*d*]thiazole), 127.6 (CH$_3$-<u>Ph</u>-), 129.0 (-<u>Ph</u>-

NH-), 134.6 (CH_3-Ph-), 134.8 (-benzo[*d*]thiazole), 134.9 (CH_3-Ph-), 149.1 (-Ph-NH-), 152.4 (CH_3-Ph-), 153.4 (-benzo[*d*]thiazole), 167.3 (-benzo[*d*]thiazole), 171.3 (-benzo[*d*]thiazole). MS (ES^+): 388 (MH^+). HRMS (MALDI) 388.096 (MH^+). HPLC (gradient water/CH_3CN from 100 % of water in 60 min, flow = 1 mL/min, λ = 254 nm): t_R =51.4 min.

2-(benzo[d]thiazol-2-ylmethylthio)-6-ethoxybenzo[d]thiazole (**34**). The compound 2-(chloromethyl)benzo[*d*]thiazole (1.00 g, 5.45 mmol), dissolved in THF (50 mL), was added drop-wise to a stirred solution of **4** (1.15 g, 5.45 mmol), *N*-ethyldiisopropylethylamine (1.35 mL, 8.17 mmol) and 4-dimethylaminopyridine (0.08 g, 0.54 mmol) in THF (50 mL). The reaction mixture was refluxed overnight. Then, the solution was cooled to room temperature, and water (100 mL) followed by chloroform (100 mL) were added. The organic layer was separated, washed twice in water, dried over sodium sulfate, filtered and evaporated. The crude solid was purified by column chromatography using 100% dichloromethane as an eluting solvent. The compound was obtained as dark brown solid. Yield 35% brown solid, mp 78-82 °C. ^{1}H NMR (DMSO-d_6, 200 MHz): δ 1.34 (t, 3H, *J*=6.9 Hz, -Ph-OCH_2CH_3), 4.05 (q, 2H, *J*=7.0 Hz, -Ph-OCH_2CH_3), 5.09 (s, 2H, -SCH_2-benzo[*d*]thiazole), 7.04 (dd, 1H, *J*=2.5, 6.4 Hz, -SCH_2-benzo[*d*]thiazole), 7.38-7.54 (m, 2H, -SCH_2-benzo[*d*]thiazole), 7.60 (d, 1H, *J*=2.4 Hz, -Ph-OEt), 7.76 (d, 1H, *J*=9.0 Hz, -Ph-OEt), 7.95-8.06 (m, 2H, -Ph-OEt). ^{13}C NMR (DMSO-d_6, 50 MHz): δ 14.9 (-Ph-OCH_2CH_3), 34.9 (-SCH_2-benzo[*d*]thiazole), 64.0 (-Ph-OCH_2CH_3), 105.8 (-Ph-OEt), 115.9 (-Ph-OEt), 122.2 (-SCH_2-benzo[*d*]thiazole), 122.6 (-SCH_2-benzo[*d*]thiazole), 122.8 (-Ph-OEt), 125.6 (-SCH_2-benzo[*d*]thiazole), 126.6 (-SCH_2-benzo[*d*]thiazole), 136.8 (-Ph-OEt, -SCH_2-benzo[*d*]thiazole), 147.0 (-Ph-OEt, -SCH_2-benzo[*d*]thiazole), 156.4 (-Ph-OEt), 161.5 (OEt-benzo[*d*]thiazole), 168.4 (-CH_2-benzo[*d*]thiazole). MS (ES^+): 359 (MH^+). HPLC (gradient water/CH_3CN from 100 % of water in 60 min, flow = 1 mL/min, λ = 254 nm): t_R =60.0 min.

Molecular modeling

Pharmacophore models

The first pharmacophore model was generated from compound PT-1 using a Common Feature Pharmacophore Generation Procedure as implemented in Catalyst/HipHop which is part of the Discovery Studio (DS) V3.5 suit of programs (*Accelrys Software Inc., Discovery Studio Modeling Environment, Release 3.5, San Diego: Accelrys Software Inc., 2012*). Prior to pharmacophore generation, compound PT-1 was subjected to a conformational search procedure using the CHARmm force field and the poling algorithm as implemented in the Catalyst/BEST procedure. 255 conformations were generated within an energy cutoff of 20.0 Kcal/mol and the lowest energy one was used as input to the pharmacophore generation procedure. For hypothesis generation, the following chemical functions were selected in the feature directory of Catalyst: hydrogen bond acceptor, hydrogen bond donor, aromatic ring and hydrophobic groups. Compounds were fitted to this model by using the Ligand Pharmacophore mapping protocol as implemented in DS. Briefly, compounds were subjected to a conformational search procedure as described above and the resulting conformations were subsequently fitted into the pharmacophore model using a flexible fitting method while setting the maximum omitted features parameter of 3. Fit values were obtained according to equation 1 and compared to the biological activity of these compounds.

(1) $$FitValue = \sum W\left[1 - \sum\left(\frac{D}{T}\right)^2\right]$$

Where W is a weight factor, D is the displacement of the feature from the center of the location constraint and T is the radius of the location constraint sphere for the feature.

and compared to the biological activity of these compounds.

The second pharmacophore model was generated from the three most active compounds (**29**, **33** and **34**) using a Common Feature Pharmacophore Generation procedure as implemented in DS V3.5. Catalyst/Best method with energy threshold of 20.0 Kcal/mol was chosen for conformation generation. Two inactive compounds (**25** and **31**) were selected for refinement of the pharmacophore hypothesis. Refinement was performed by setting higher weights (10) to the features that are missing in the inactive compounds but which are present in the active ones. These features include a hydrogen bond acceptor

located on the linker between two benzothiazole moieties and a hydrogen bond acceptor located on the second benzothiazole moiety. The ligand pharmacophore mapping protocol was used for mapping the set of 31 ligands considered in this work to the pharmacophore model described above while employing the flexible fitting method and setting a maximum of two omitted features. The resulting fit values were compared to the biological activity of the ligands.

Docking simulations

The structure of AMPK was downloaded from the PDB (2Y94) and prepared for docking simulations using the prepare protein module implemented in DS. Structures of PT1 and of compound **34** were drawn in ChemDraw and prepared for docking using the LigPrep procedure as implemented in Maestro (*Maestro, version 9.3, Schrodinger, LLC, New York, NY, 2012*). Docking was performed using the induced fit procedure (IFD) as implemented in Maestro which combines docking by Glide with sidechain optimization performed by Prime. In the present study we used extra precision (XP) docking with the OPLS2005 force field. All other IFD parameters were kept at their default values. The docking box was positioned at the vicinity of residues Glu 94 and Lys 154 in accord with the position of PT1 within the AMPK binding site as previously suggested by Pang et al. [20]

Animals

Diabetic male KKAy mice (8 to 12-week old, 20-25 g) were purchased from The Jackson Laboratory (Bar Harbor, ME). The animals were routinely kept in 12-h light/dark cycles and provided with food and water *ad libitum*. Blood glucose levels at sacrifice ranged between 17-25 mmol/l. The ethics committee of the Hebrew University of Jerusalem approved the study protocol for animal welfare. The Hebrew University of Jerusalem is an Association for Assessment and Accreditation of Laboratory Animal Care (AAALAC) international accredited institution.

Intraperitoneal Glucose Tolerance Test (ip-GTT)

A standard ip-GTT test was performed on mice after an overnight fast. Glucose in saline was injected ip (1.5 g/kg body weight). Venous blood samples from small tail clips were taken for glucose determination using a glucometer (FreeStyle Freedom, Abbott Diabetes Care, Alamada, CA).

L6 myotube cultures

L6 myotubes were maintained as previously described.[39] All experiments were conducted on fully differentiated myotubes.

2-[^{3}H,1]-Deoxy-D-glucose uptake assay

The rate of [^{3}H]dGlc uptake in myotubes, in the absence or presence of insulin, was determined as previously described.[7] Briefly, L6 myotube cultures were preincubated in α-MEM supplemented with 2% (v/v) FCS and 23.0 mmol/L. D-glucose for 24 h, and then 4 h before the experiment the medium was changed to serum-free medium with 0.5% BSA. The myotubes were then treated as described in Fig. 1. The insulin effect was measured after its addition (200 nmol/L) to cultures for the last 30 min of treatment. The cultures were then rinsed 3 times with PBS at room temperature and incubated with PBS, pH 7.4, containing 0.1 mmol/L dGlc and 1.3 μCi/mL [^{3}H]dGlc for 5 min at room temperature. At the end of the assay, the myotubes were lysed in 0.1% (w/v) SDS in water and taken for liquid scintillation.

Preparation of cell lysates and WB (Western blot) analysis

Whole cell lysates were prepared as previously described[7] with some minor modifications: the lysis buffer contained 50 mmol/L Tris-HCl, pH 7.5, 1 mmol/L EDTA, 1mmol/L EGTA, 1 mmol/L Na_3VO_4, 150 mmol/L NaCl, 50 mmol/L NaF, 10 mmol/L sodium-glycerophosphate, 5 mmol/L sodium pyrophosphate, and 1 mmol/L PMSF, supplemented with 0.1% (v/v) NP-40, 0.1% (v/v) 2-β-mercaptoethanol, and protease inhibitor cocktail (1:100 dilution). The cells were washed with ice-cold PBS, and 1 mL of lysis buffer was then added and incubated at 4 °C for 40 min. The resulting cell lysates were centrifuged at 8,700 *g* x 30 min at 4 °C and the resulting supernatant fractions were

separated and kept at -20 °C until used. Protein content in the supernatant was determined according to Bradford [40], using a BSA standard dissolved in the same buffer. Aliquots (5-60 μg of protein) were mixed with the sample buffer [62.5 mmol/L Tris-HCl, pH 6.8, 2% (w/v) SDS, 10% (v/v) glycerol, 50 mmol/L DTT, and 0.01% (w/v) bromophenol blue], heated at 95°C for 5 min. Samples for WB analyses of GLUT1 and GLUT4 were prepared as previously described. [41] The proteins were separated on 10% SDS-PAGE and WB analyses were performed using antibodies according to our previously established protocols.

Colorimetric determination of surface GLUT1myc and GLUT4myc in L6 myotubes

The colorimetric detection of surface GLUT4myc or GLUT1myc in L6 myotubes was performed as described. [33] Briefly, cultured myotubes were incubated with rabbit anti-c-Myc antibody (1:200 dilution), washed and fixed with 3% formaldehyde, and further interacted with goat HRP-conjugated anti-rabbit IgG (1:2000 dilution). Following the washes, a solution of OPD was added, and the culture plates were taken for absorbance measurement at 492 nm to estimate the relative abundance of GLUT1myc or GLUT4myc on the plasma membrane of the myotubes. The GLUT1myc and GLUT4myc L6 cells were the courtesy of Dr. A. Klip, Hospital for Sick Children (Toronto, ON, Canada).

Colorimetric determination of cellular ATP level in L6 myotubes

ATP content in lysates of L6 myotubes was measured with the ATP assay kit. A **34**, DMSO and known uncoupler dinitrophenol (DNP) as a positive control were added to L6 myotubes for indicate din the Table 3 times. Myotubes in 6-well plates were washed 3 times with cold 0.15 M Tris HCl, pH 7.75. The wells were then treated with 200 μL of 0.5% (w/v) ice-cold TCA, followed by the addition of 400 μL of Tris-HCl buffer. The mixture was centrifuged in Eppendorf tubes (12,000 rpm, 30 min at 4 °C) and the supernatant taken for ATP determination according to the manufacturer's instructions. The assay was performed in 96-multi-well plates (Nunc, Roskilde, Denmark) in an EXx800 spectrophotometer (Biotec

Instruments, Winooski, VT) at room temperature. ATP standard curve was constructed according to the manufacturer's protocol, using the ATP supplied in the kit.

LogP calculations

Theoretical LogP values were calculated using Advanced Chemistry Development (ACD/Labs) Software V11.02 (© 1994-2012 ACD/Labs). The experimental LogP/D for **34** was determined as described in SI.

Statistical analysis

Results are given as Mean ± SEM. Statistical significance ($p<0.05$) was calculated among experimental groups using the two-tailed Student's t test. The http://www.graphpad.com/quickcalcs/ttest1.cfm online service was used for statistical evaluations.

ACKNOWLEDGMENTS

This study was supported partly by a Bar-Ilan University new faculty grant and the EFSD/D-Cure Program for Young Investigator Awards for Collaborative Diabetes Research between Israel and Europe (to A.G and J.E). This study was also supported by Diab R&D (France) and grants from the Applied Research Program A of the Hebrew University, and the Israel Science Foundation of The Israel Academy of Sciences and Humanities (to S.S). S. Sasson is member of the David R. Bloom Center for Pharmacy and the Dr. Adolf and Klara Brettler Center for Research in Molecular Pharmacology and Therapeutics, and the Adolf D. and Horty Storch Chair in Pharmaceutical Sciences, Faculty of Medicine, The Hebrew University of Jerusalem. We thank Ms. Duha Fahham and Mr. Yosef Avrahami for their technical help in conducting glucose uptake assays. We are thankful to Dr. Rachel Persky for the MS analysis, to biochemistry department of Enamine Ltd. for performing the biostability studies and to Mr. Yosef Mackler for editing the manuscript.

SUPPORTING INFORMATION

Supporting Information Available: supportive biological data, results of biostability of **34**, analytical data of synthesized compounds and molecular modeling fit values/calculations. This material is available free of charge via the Internet at http://pubs.asc.org.

Corresponding Authors: *A.G.: email: gruzmaa@biu.ac.il, Phone: +972-3-7384597, Fax: +972-3-738-4053; *S.S. shlomo.sasson@mail.huji.ac.il, Phone +972-2-576-8798, Fax:+972-2-675-8741

ABBREVIATION LIST

AAALAC, Association for Assessment and Accreditation of Laboratory Animal Care;

ACC, Acetyl CoA Carboxylase;

AICAR, 5-Aminoimidazole-4-carboxamide-1-β-D-ribofuranoside;

ADA, American Diabetes Association;

AMPK, AMP-activated protein kinase;

AS-160, AMPK substrate 160 kDa;

GTT, glucose tolerance test;

dGlc, 2-deoxy-D-glucose;

DNP, Dinitrophenol;

DS, Discovery Studio;

EDC, 3-(ethyliminomethyleneamino)-*N*,*N*-dimethyl-propan-1-amine;

EASD, European Association for the Study of Diabetes;

FCS, fetal calf serum;

GLUT, glucose transporter;

HCGM, High concetration glucose medium: 23.0 mmol/L D-Glucose;

HOBt, 1-hydroxybenzotriazole;

HRP, horseradish peroxidase;

KKAy, Kuo Kondo rats carrying the Ay yellow obese gene;

αMEM, alpha-Minimal essential medium;

MTT, (3-(4,5-Dimethylthiazol-2-yl)-2,5-diphenyltetrazolium bromide test

OPD, O-phenylenediamine;

PI3K, Phosphatidylinositide 3-Kinase;

PMSF, phenylmethanesulfonylfluoride;

WB, Western Blot

FIGURE CAPTIONS

Figure 1. Compounds **3, 4** and **15** increase the rate of glucose uptake in L6 myotubes by activating AMPK.

Figure 2. Compounds **24, 29, 33** and **34** increase the rate of glucose uptake in L6 myotubes by activating AMPK.

Figure 3. Compound **34** induces GLUT4 translocation to the plasma membrane of L6 myotubes in a non-insulin-dependent manner and stimulates phosphorylation of AMPK downstream targets.

Figure 4. Antihyperglycemic effects of **34** in diabetic KKAy mice.

Figure 5. PT-1 based pharmacophore model.

Figure 6. The pharmacophore model generated based on the compounds synthesized in the present work.

Figure 7. Binding modes of PT1 and compound **34** to AMPK.

SCHEME TITLES

Scheme 1. Synthesis of **20**-**27** and **33**.

Scheme 2. Synthesis of **29** and **30**.

Scheme 3. Synthesis of **31**, **32** and **34**.

CHART TITLES

Chart 1. Determination of possible minimal active moiety of PT-1.

Table 1

Compound	Structure	Effect on glucose uptake [100µM] in L6 myotubes (%)	EC_{50} [µM]	Phosphorylation of AMPK at Thr^{172}
3 2-amino-5-ethylthiazol-4(5H)-one	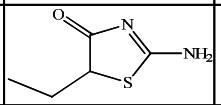	134.9±11.4*	61.5±4.3	+
5 2-amino-1,3,4-thiadiazole	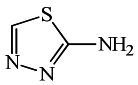	97.4±2.9	-	-
6 2-amino-5-methyl-1,3,4-thiadiazole	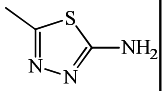	101.4±5.5	-	-
7 3-mercapto-4-methyl-4H-1,2,4-triazole	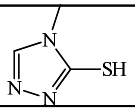	107.0±7.5	-	-
8 2-mercaptopyrimidine	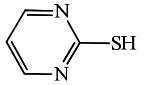	100.5±4.9	-	-
9 2-mercapto-1-methylimidazole	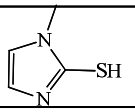	93±9.5	-	-
10 2-aminothiazole	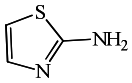	95.7±5.1	-	-
11 2-mercapto-2-thiazoline	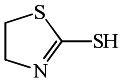	105.6±6.8	-	-
12 2-amino-5-nitrothiazole	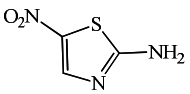	95.1±8.9	-	-

(n=6, for the glucose uptake measurement, n=3 for WB analysis).

Table 2

Compound	Structure	Effect on glucose uptake [100µM] in L6 myotubes (%)	EC_{50} [µM]	Phosphorylation of AMPK at Thr^{172}
4 6-ethoxybenzo[d]thiazole-2-thiol	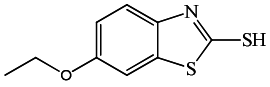	179.1±9.5*	76.1±9.4	+
13 benzothiazole	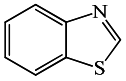	117.4±9.7	-	-
14 6-ethoxybenzothiazol-2-amine	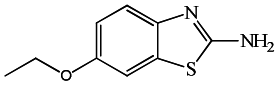	111.4±14.2	-	-
15 6-bromo-2-benzothiazolinone	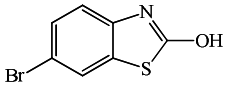	144.1±8.8*	72.9±6.4	+
16 1H-1,2,3-triazolo[4,5]pyridine	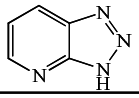	86.7±17.9	-	-
17 1H-benzotriazole	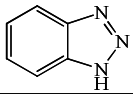	87.5±11.4	-	-
18 benzothiazol-2-amine	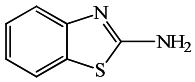	95.7±5.1	-	-

(n=6, for the glucose uptake measurement, n=3 for WB analysis).

Table 3.

INCUBATION CONDITION	ATP (mmol/mg protein)
5.0 mmol/L D-Glucose	1.24 ± 0.07
23.0 mmol/L D-Glucose (High concetration glucose medium, HCGM)	1.31 ± 0.09
HCGM + DMSO (0.1 %, v/v)	1.42 ± 0.05
HCGM + **34** (5 μM)	1.32 ± 0.04
HCGM + **34** (25 μM)	1.31 ± 0.02
HCGM + **34** (100 μM)	1.30 ± 0.05
HCGM + **34** (200 μM)	1.28 ± 0.07
HCGM + DNP (3.5 mmol/L, 20 min)	0.42 ± 0.1*

Cellular levels of ATP in L6 myotubes following treatment with **34**. L6 myotubes were preconditioned with the indicated glucose concentration and treated with various concentrations of **34** for 5 h, as described in the legend to Figure 3. At the end of incubation the myotubes were lysed and the ATP content was determined as described under *Experimental section*. *p<0.05, in comparison with the untreated cells in 23.0 mmol/L D-glucose concentration in the medium.

REFERENCES

(1) Bouzakri, K.; Koistinen, H.A.; Zierath, J. R. Molecular mechanisms of skeletal muscle insulin resistance in type 2 diabetes. *Curr. Diabetis Rev*. **2005**, *1*, 167-174.

(2) Ferrannini, E. Is insulin resistance the cause of the metabolic syndrome? *Ann. Med*. **2006**, *38*, 42-51.

(3) Del Prato, S., Matsuda, M., Simonson, D.C., Groop, L.C., Sheehan, P., Leonetti, F., Bonadonna, R.C., DeFronzo, R.A. Studies on the mass action effect of glucose in NIDDM and IDDM: evidence for glucose resistance. *Diabetologia*. **1997,** *40,* 687-697.

(4) Rothman, D.L., Magnusson, I., Cline, G., Gerard, D., Kahn, C.R., Shulman, R.G., Shulman, G.I. Decreased muscle glucose transport/phosphorylation is an early defect in the pathogenesis of non-insulin-dependent diabetes mellitus. *Proc. Natl. Acad. Sci. U S A*. **1995**, *92*, 983-987.

(5) Sasson, S., Ashab, Y., Melloul, D., Cerasi, E. Autoregulation of glucose transport: effects of glucose on glucose transporter expression and cellular location in muscle. *Adv. Exp. Med. Biol,* **1993**, *334* 113-127.

(6) Gruzman, A., Elgart, A., Viskind, O., Billauer, H., Dotan, S., Cohen, G., Mishani, E., Hoffman, A., Cerasi, E., Sasson, S. Antihyperglycaemic activity of 2,4:3,5-dibenzylidene-D-xylose-dithioacetal in diabetic mice. *J. Cell Mol. Med*. **2011**, *16*, 593-603.

(7) Gruzman, A., Shamni, O., Ben Yakir, M., Sandovski, D., Elgart, A., Alpert, E., Cohen, G., Hoffman, A., Katzhendler, Y., Cerasi, E., Sasson, S. Novel D-xylose derivatives stimulate muscle glucose uptake by activating AMP-activated protein kinase alpha. *J. Med. Chem*. **2008,** *51,* 8096-8108.

(8) Sasson, S., Edelson, D., Cerasi, E. In vitro autoregulation of glucose utilization in rat soleus muscle. *Diabetes*, **1987,** *36,* 1041-1046.

(9) Sasson, S., Cerasi, E. Substrate regulation of the glucose transport system in rat skeletal muscle. Characterization and kinetic analysis in isolated soleus muscle and skeletal muscle cells in culture. J. Biol. Chem. **198**6, *261,* 16827-16833.

(10) Stump, C.S., Henriksen, E.J., Wei, Y., Sowers, J.R. The metabolic syndrome: role of skeletal muscle metabolism. *Ann. Med*. **2006**, *38*, 389-402.

(11) Kahn, B.B., Flier, J.S. Regulation of glucose-transporter gene expression in vitro and in vivo. *Diabetes Care*, **1990**, *13,* 548-564.

(12) Fujii, N., Jessen, N., Goodyear, L.J. AMP-activated protein kinase and the regulation of glucose transport. *Am. J. Physiol. Endocrinol. Metab*. **2006**, *291*, E867-E877.

(13) Koh, H.J., Brandauer, J., Goodyear, L.J. LKB1 and AMPK and the regulation of skeletal muscle metabolism. *Curr. Opin. Clin. Nutr. Metab. Care*. **2008**, *11,* 227-232.

(14) Hardie, D.G. Energy sensing by the AMP-activated protein kinase and its effects on muscle metabolism. *Proc. Nutr. Soc.* **2011,** *70,* 92-99.

(15) Dzamko, N.L., Steinberg, G.R. AMPK-dependent hormonal regulation of whole-body energy metabolism. *Acta Physiol (Oxf)*. **2009**, *196,* 115-127.

(16) Zhang, B.B., Zhou, G., Li, C. AMPK: an emerging drug target for diabetes and the metabolic syndrome. *Cell Metab.* **2009,** *9,* 407-416.

(17) Yun, H., Ha, J. AMP-activated protein kinase modulators: a patent review (2006 - 2010). *Expert Opin. Ther. Pat.* **2011**, *21,* 983-1005.

(18) Gruzman, A., Babai, G., Sasson, S. Adenosine monophosphate-activated protein kinase (AMPK) as a new target for antidiabetic drugs: A review on metabolic, pharmacological and chemical considerations. *Rev. Diab. Stud.* **2009,** *6,* 13-36.

(19) Inzucchi, S.E., Bergenstal, R.M., Buse, J.B., Diamant, M., Ferrannini, E., Nauck, M., Peters, A.L., Tsapas, A., Wender, R., Matthews, D.R. Management of hyperglycaemia in type 2 diabetes: a patient-centered approach. Position statement of the American Diabetes Association (ADA) and the European Association for the Study of Diabetes (EASD). *Diabetologia*. **2012,** 55, 1577-1596.

(20) Pang, T., Zhang, Z.S., Gu, M., Qiu, B.Y., Yu, L.F., Cao, P.R., Shao, W., Su, M.B., Li, J.Y., Nan, F.J., Li, J. Small molecule antagonizes autoinhibition and activates AMP-activated protein kinase in cells. J. Biol. Chem. **2008**, *283*, 16051-16060.

(21) Woltersdorf Jr, O.W., Schwam, H., Bicking, J.B., Brown, S.L., DeSolms, S.J., Fishman, D.R., Graham, S.L., Gautheron, P.D., Hoffman, J.M. Topically active carbonic anhydrase inhibitors. 1. O-acyl derivatives of 6-hydroxybenzothiazole-2-sulfonamide. *J. Med. Chem,* **1989**, *32*, 2486-2492.

(22) Oprea, T.I. Current trends in lead discovery: are we looking for the appropriate properties? *Mol Divers.* **2002,** *5,* 199-208.

(23) Nagahara, N., Matsumura, T., Okamoto, R., Kajihara, Y. Protein cysteine modifications: (1) medical chemistry for proteomics. *Curr. Med. Chem.* **2009,** *16,* 4419-4444.

(24) Schoenwald, R.D, Eller, M.G., Dixson, J.A., Barfknecht, C.F.Topical Carbonic Anhydrase Inhibitors. *J. Med.Chem.* **1984,** *27,* 810-812.

(25) Olsen, R.K., Apparao, S., Bhat, K.L. Synthesis of a model analogue of the cyclic decadepsipeptide intercalating agent luzopeptin A (antibiotic BBM 928A) containing proline, valine, and unsubstituted quinoline substituents. *J. Org. Chem.* **1986,** *51,* 3079-3085.

(26) Wu, X., Motoshima, H., Mahadev, K., Stalker, T.J., Scalia, R., Goldstein, B.J. Involvement of AMP-activated protein kinase in glucose uptake stimulated by the globular domain of adiponectin in primary rat adipocytes. *Diabetes*. **2003,** *52,* 1355-1363.

(27) Hopkins, T.A., Dyck, J.R., Lopaschuk, G.D. AMP-activated protein kinase regulation of fatty acid oxidation in the ischaemic heart. *Biochem. Soc. Trans.* **2003**, *31,* 207-212.

(28) Ruderman, N.B., Dean, D. Malonyl CoA, long chain fatty acyl CoA and insulin resistance in skeletal muscle. *J. Basic Clin. Physiol. Pharmacol.* **1998,** *9,* 295-308.

(29) Holt, P.S., Buckley, S., Deloach, J.R. Detection of the lethal effects of T-2 mycotoxin on cells using a rapid colorimetric viability assay. *Toxicol. Lett.* **1987,** *39,* 301-312.

(30) Narayanan, B., Islam, M.N., Bartelt, D., Ochs, R.S. A direct mass-action mechanism explains capacitative calcium entry in Jurkat and skeletal L6 muscle cells. *J. Biol. Chem.* **2003**, 278, 44188-44196.

(31) Klip, A., Schertzer, J.D., Bilan, P.J., Thong, F., Antonescu, C. Regulation of glucose transporter 4 traffic by energy deprivation from mitochondrial compromise. *Acta Physiol. (Oxf)*. **2009,** *196*, 27-35.

(32) Carling, D., Mayer, F.V., Sanders, M.J., Gamblin, S.J. AMP-activated protein kinase: nature's energy sensor. *Nat. Chem. Biol.* **2011,** *18,* 512-518.

(33) Wang, Q., Khayat, Z., Kishi, K., Ebina, Y., Klip, A. GLUT4 translocation by insulin in intact muscle cells: detection by a fast and quantitative assay. *FEBS Lett.* **1998,** *427,* 193-197.

(34) Baragli, A., Ghè, C., Arnoletti, E., Granata, R., Ghigo, E., Muccioli, G. Acylated and unacylated ghrelin attenuate isoproterenol-induced lipolysis in isolated rat visceral adipocytes through activation of phosphoinositide 3-kinase γ and phosphodiesterase 3B. *Biochim. Biophys. Acta.* **2011,** *1811,* 386-396.

(35) Iwatsuka, H., Shino, A., Suzuoki, Z. General survey of diabetic features of yellow KK mice, *Endocrinol. Jpn*. **1970**, *17*, 23-35.

(36) Gottlieb, H.E., Kotlyar, V., Nudelman, A. NMR chemical shifts of common laboratory solvents as trace impurities. *J. Org. Chem*. **1997**, *62*, 7512-7515.

(37) Banwell, M.G., McRae, KJ. A chemoenzymatic total synthesis of ent-Bengamide E. *J. Org. Chem.* **2001,** *66,* 6768-6774.

(38) Russell, M.G., Carling, R.W., Atack, J.R., Bromidge, F.A., Cook, S.M., Hunt, P., Isted, C., Lucas, M., McKernan, R.M., Mitchinson, A., Moore, K.W., Narquizian, R., Macaulay, A.J., Thomas, D., Thompson, S.A., Wafford, K.A., Castro, J.L. Discovery of functionally selective 7,8,9,10-tetrahydro-7,10-ethano-1,2,4-triazolo[3,4-a]phthalazines as GABA A receptor agonists at the alpha3 subunit. J. Med. Chem. **2005**, *48*, 1367-1383.

(39) Braverman, S. Cherkinsky, M. Kalendar, Y. Gottlieb, H. Meltzer-Mats, E. Gruzman, A. Goldberg, I. Sprecher, M. One-pot three-component preparation of novel selenium-containing spiroketals. J. Phys. Org. Chemistry. **2013**, *26*, 102-108.

(40) Bradford, M.M. A rapid and a sensitive method for the quantitation of microgram quantities of protein utilizing the principle of protein dye binding. *Anal. Biochem.* **1972,** *72,* 248–254.

(41) Sasson, S., Gorowits, N., Joost, H.G., King, G.L., Cerasi, E., Kaiser, N. Regulation by metformin of the hexose transport system in vascular endothelial and smooth muscle cells. *Br. J. Pharmacol*. **1996**, *117*, 1318-1324.

Figures, Schemes and Chart

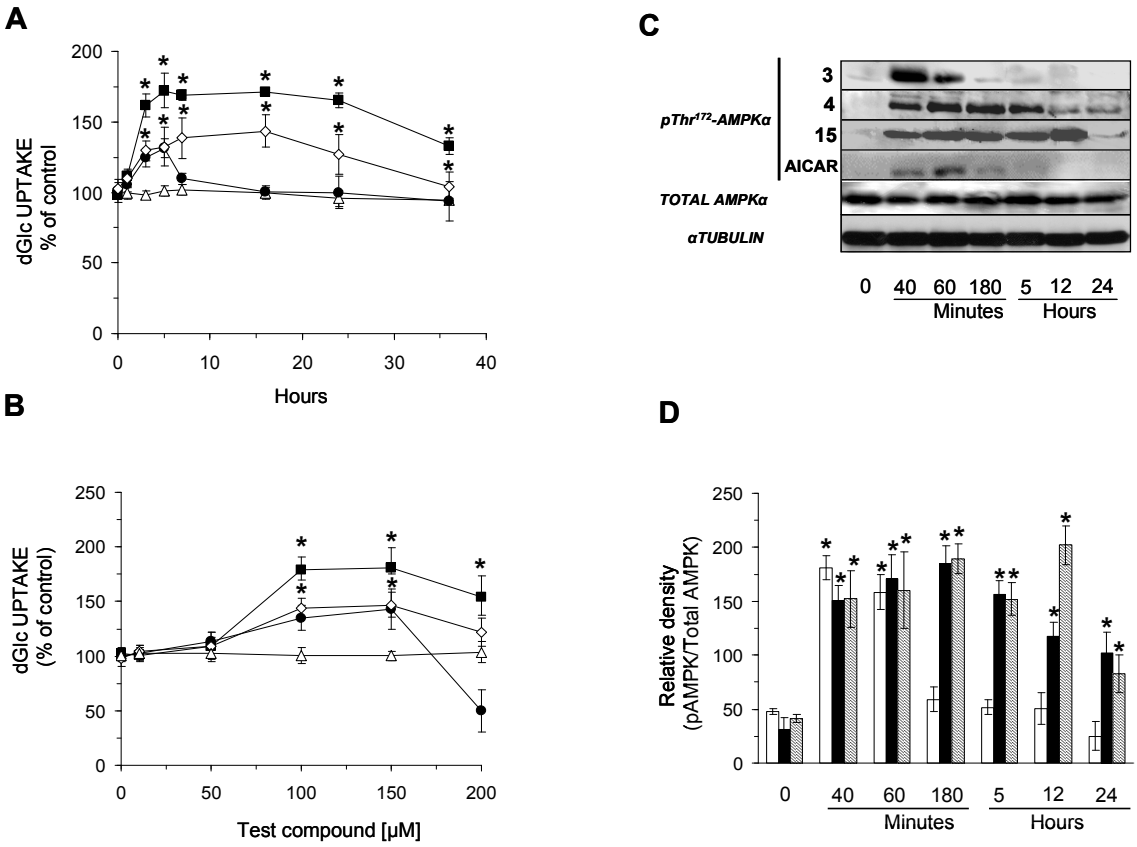

Figure 1

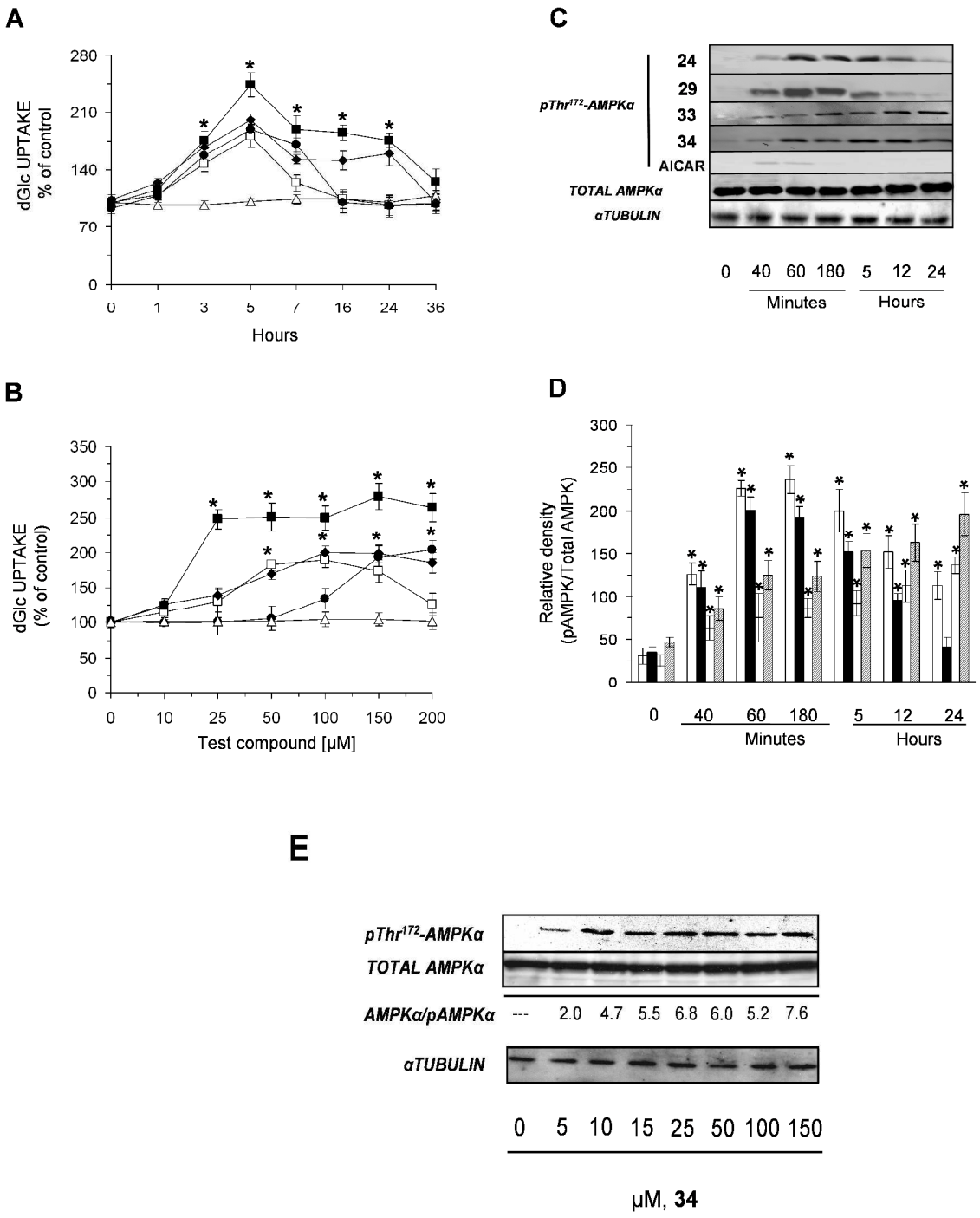
A
dGlc UPTAKE
% of control
280
210
140
70
0
0 1 3 5 7 16 24 36
Hours
B
dGlc UPTAKE
(% of control)
350
300
250
200
150
100
50
0
0 10 25 50 100 150 200
Test compound [μM]
C
pThr172-AMPKα
24
29
33
34
AICAR
TOTAL AMPKα
αTUBULIN
0 40 60 180 5 12 24
Minutes
Hours
D
Relative density
(pAMPK/Total AMPK)
300
250
200
150
100
50
0
0 40 60 180 5 12 24
Minutes
Hours
E
pThr172-AMPKα
TOTAL AMPKα
AMPKα/pAMPKα --- 2.0 4.7 5.5 6.8 6.0 5.2 7.6
αTUBULIN
0 5 10 15 25 50 100 150
μM, 34

Figure 2

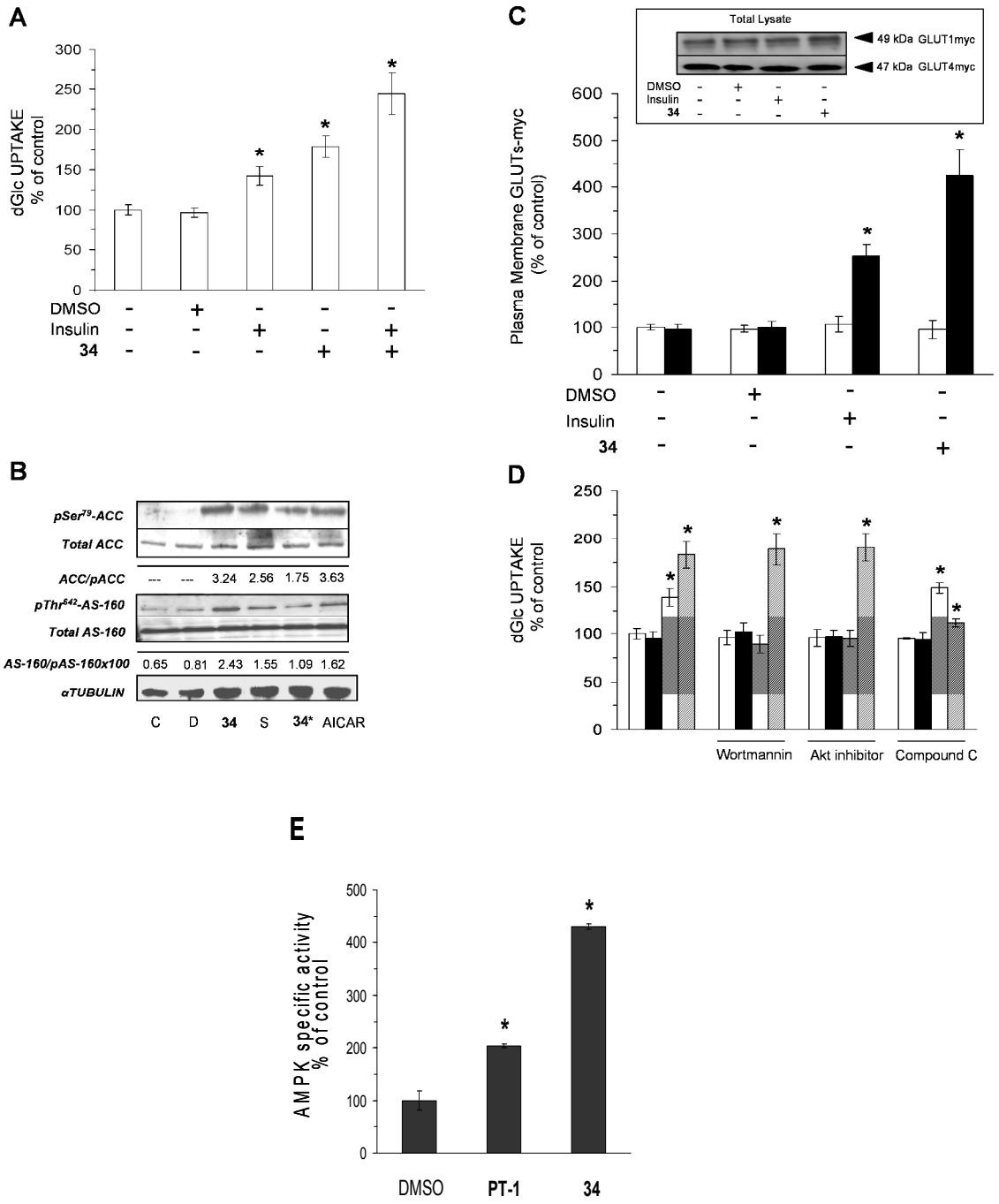
A
dGlc UPTAKE
% of control
DMSO
Insulin
34
B
pSer79-ACC
Total ACC
ACC/pACC
3.24 2.56 1.75 3.63
pThr642-AS-160
Total AS-160
AS-160/pAS-160x100
0.65 0.81 2.43 1.55 1.09 1.62
αTUBULIN
C D 34 S 34* AICAR
C
Total Lysate
49 kDa GLUT1myc
47 kDa GLUT4myc
Plasma Membrane GLUTs-myc
(% of control)
D
dGlc UPTAKE
% of control
Wortmannin
Akt inhibitor
Compound C
E
AMPK specific activity
% of control
DMSO
PT-1
34

Figure 3

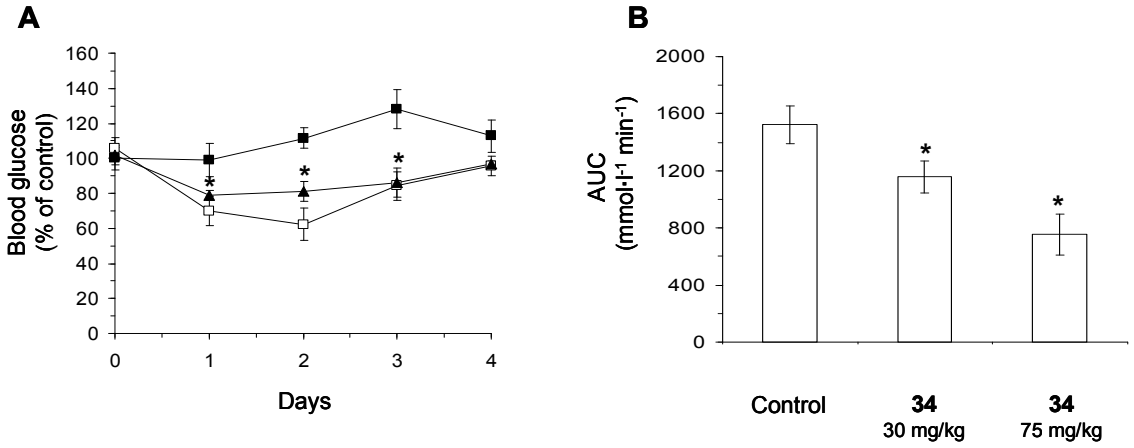

Figure 4

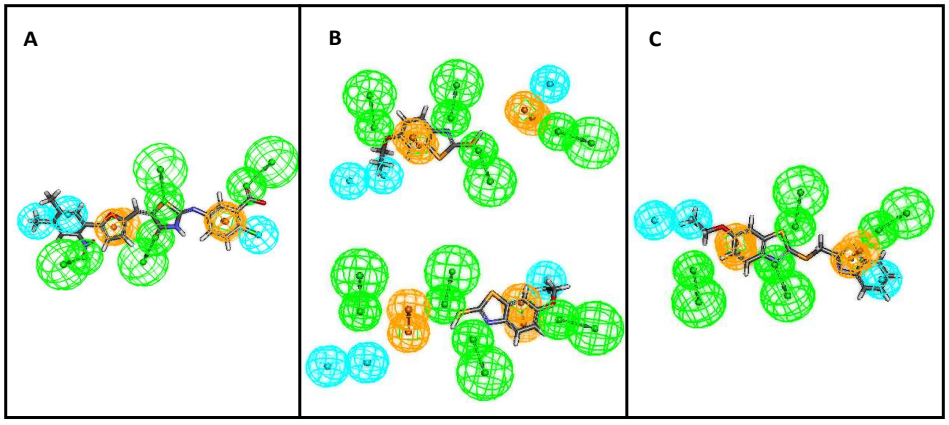

Figure 5

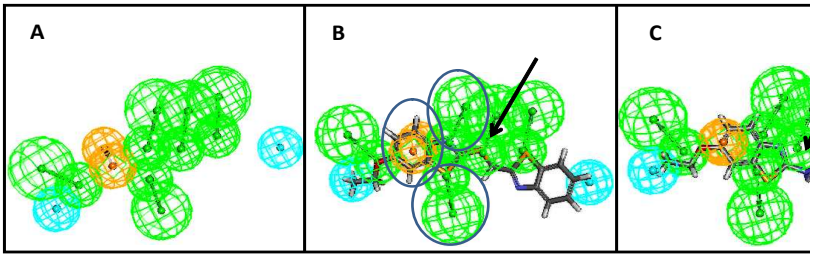

Figure 6

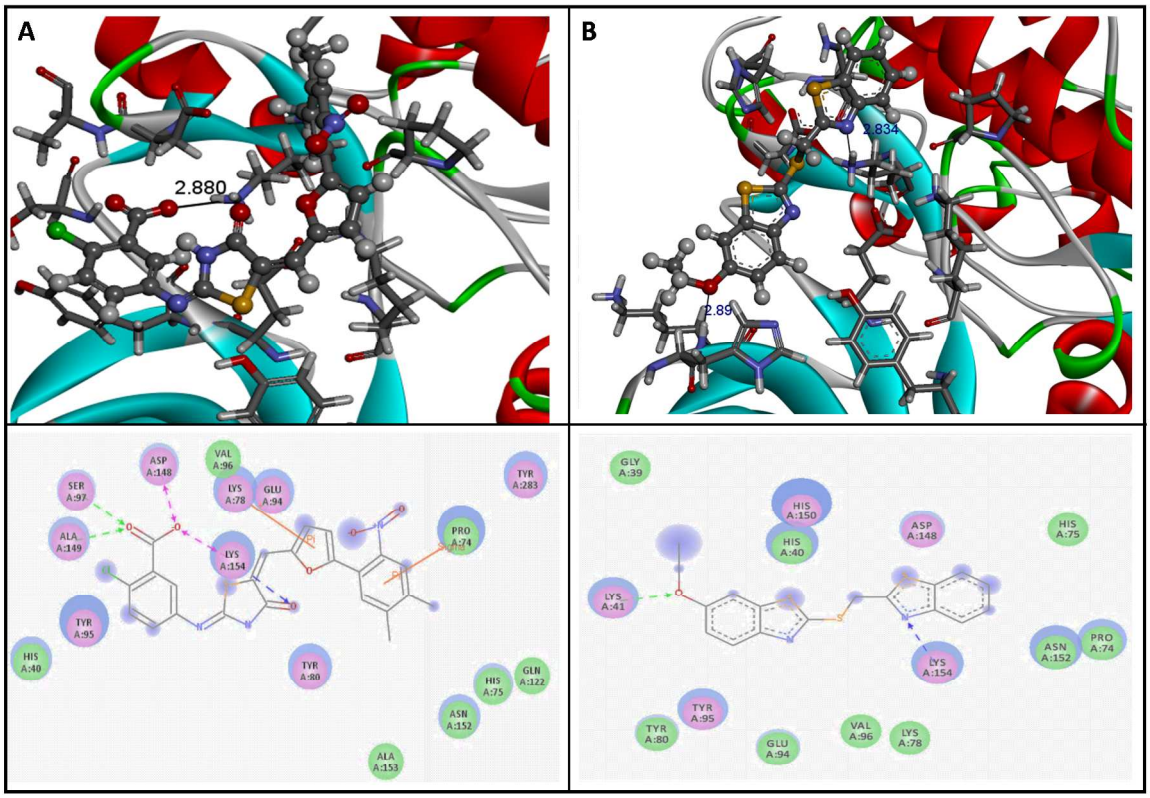

Figure 7

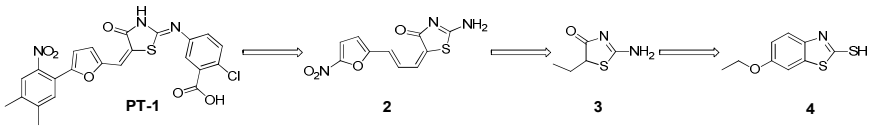

Chart 1

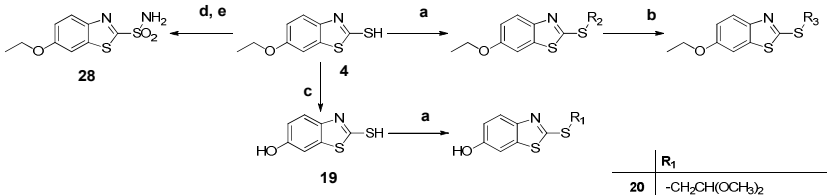

	R_1
20	$-CH_2CH(OCH_3)_2$
21	$-CH_2CH(CH_2CH_3)_2$
22	$-CH_2CH_2CH_2CH_3$
	R_2
23	$-CH_2CO_2H$
24	$-CH_2CH_2CO_2H$
25	$-CH_2CH_2CH_3$
26	$-CH_2CH(CH_2CH_3)_2$
27	$-CH_2CH_2CH_2CH_3$
	R_3
33	$-CH_2-CONH-CH_2CH_2CH_3$

Scheme 1

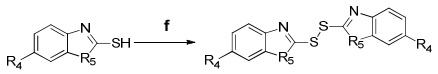

	R_4	R_5
29	$-OCH_2CH_3$	-S
30	-H	-NH

Scheme 2

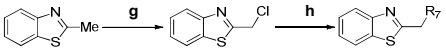

	R_7
31	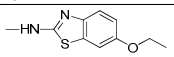
32	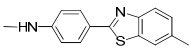
34	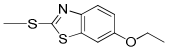

Scheme 3

Figure and Scheme legends

Figure 1. (**A**) Time-course analysis: myotube cultures were washed and received fresh αMEM supplemented with 2% (v/v) FCS, 23.0 mM D-glucose and 100 μM of **3** (●), **4** (■) or **15** (◊); they were incubated for the indicated time periods. Control myotubes received the vehicle (DMSO) only (Δ). The cultures were then taken for the dGlc uptake assay. The basal rate of [^{3}H]dGlc uptake at the beginning of the experiment (2.28±0.1 nmol/mg protein/min) was assigned the 100% value. (**B**) Dose response analysis: myotube cultures were incubated with the indicated concentrations of **3** (●, 5 h), **4** (■, 12 h) or **15** (◊, 12 h). Control myotubes received the vehicle only (Δ). All cultures were incubated for 5 and 12 h, then washed and taken for the standard [^{3}H]dGlc uptake assay. The basal rate of dGlc uptake at zero time (2.38±0.21 nmol/mg protein/min) was taken as 100%. (**C**) AMPK activation: L6 myotube cultures were treated with 100 μM of **3**, **4**, **15**, or 4 mM AICAR for the indicated times. Whole cell lysates were prepared and WB analyses performed with antibodies against pThr^{172}-AMPKα, AMPKα and α-tubulin. Representative blots are shown. AMPKα and α-tubulin blots shown only for with **3** treated myotubes. Level of these two proteins was unchanged in **4**, **15** and AICAR treated cells. (**D**) Summary of the band density measurements of three independent experiments of Compound **3** (open bars), **4** (black bars) and **15** (hatched bars). *$p<0.05$, in comparison to the respective controls.

Figure 2. (**A**) The time-course analysis was conducted as described in the legend to Figure 1: L6 myotubes were exposed to 50 μM of **24** (□), 150 μM of **29** (●), 100 μM of **33** (♦) or 25 μM of **34** (■). Control myotubes received the vehicle (DMSO) only (Δ). The basal rate of [^{3}H]dGlc uptake at zero time (1.45±0.21 nmol/mg protein/min) was taken as 100%. (**B**) Dose–response analysis: L6 myotubes were incubated with increasing concentrations of **24** (□), **29** (●), **33** (♦), **34** (■) or the vehicle (Δ) for 5 h. The basal rate of dGlc uptake at zero time (1.49±0.15 nmol/mg protein/min) was taken as 100%. (**C**) AMPK activation: L6 myotube cultures were treated with the test compounds as described in Panel A. WB analyses were performed as described in the legend to Figure 1. Representative blots are shown. AMPKα and α-tubulin blots shown only for with **24** treated myotubes. Level of these two proteins was

unchanged in **29**, **33, 34** and AICAR treated cells. (**D**) Summary of the band density measurements of three independent experiments of Compound **24** (open bars), **29** (black bars), **33** (hatched bars) and **34** (bold hatched bars). *$p<0.05$, in comparison to the respective controls. (**E**) Dose response effect of **34** on AMPK phosphorylation: L6 myotube cultures were treated with increasing concentrations of **34** (from 5 till 150 μM) for 4 h. Whole cell lysates were prepared and WB analyses performed with antibodies against pThr^{172}-AMPKα, AMPKα and α-tubulin. Representative blots are shown.

Figure 3. (**A**) Additive effects of **34** and insulin on glucose uptake in L6 myotubes: L6 myotube cultures were washed and received serum free-αMEM with 0.5% of BSA, containing 23.0 mM D-glucose and incubated for 9 h. During the last 5 h of incubation the cells received 25 μM of **34** or the vehicle DMSO (0.1% v/v). Insulin (100 nM) was introduced during the last 20 min of incubation. The basal rate of the dGlc uptake (1.62±0.1 nmol /mg protein/min) was taken as 100%. *$p<0.05$ in comparison with suitable control group. (**B**) Compound **34** activates downstream AMPK targets. The cultures were preincubated for 3 h with 5 μM Compound C prior to the addition of **34** (25 μM) for 3 h , sorbitol (250 mM) for 40 min and AICAR (4 mM) for 30 min. Whole cell lysates were prepared as described in *Experimental section*. The content of pSer^{79}-ACC, ACC, pThr^{642}-AS-160, AS-160 and α-tubulin was determined by WB analysis. Representative blot and a summary of n =3. *, $p < 0.05$, in comparison with the respective controls. (**C**) Compound **34** induces GLUT4, but not GLUT1 translocation to the plasma membrane of L6 myotubes: cells expressing GLUT1myc or GLUT4myc were treated with 25 μM of **34** or DMSO as described above. At the end of the incubation, the cultures were taken for immunodetection of surface GLUT1myc (open bars) or GLUT4myc (black bars), as described under the *Experimental section*. *$p<0.05$ in comparison with the respective control. *Inset*: representative WB analysis of the total content of the corresponding glucose transporters in whole cell lysates prepared from L6 myotubes that were treated as described above. (**D**) Compound **34** augments the rate of glucose transport in a PI3K-and Akt/PKB-independent manner: control L6 myotubes (open bars) or myotubes treated as described above with **34** (hatched bars), insulin (bold hatched bars) or the

vehicle (black bars), were incubated in the absence or presence of 100 nM of wortmannin or 100 nM of the Akt/PKB inhibitor or 5 μM of compound C. The former inhibitors were added 30 min prior to the addition of **34** or insulin to L6 myotube cultures whereas compound C was introduced to the cultures 5 h prior the uptake assay with **34**. The basal rate of the dGlc uptake (2.32±0.12 nmol/mg protein/min) in myotubes exposed to 23 mM D-glucose with DMSO was taken as 100%. (E) Compound **34** directly enhances the AMPK activity: the experiment was conducted using ADP-Glo^{tm} AMPK A1/B1/G1 kinase kit from SignalChem according to the manufacture protocol. A vehicle (DMSO, 1% v/v), PT-1 (20 μM) and **34** (20 μM) were added to the reaction mix for 30 min in ambient temperature. The signal (the calibration curve and the compounds measurement) was detected by Synergy4 Luminometer (BioTek Instruments, Winooski, VT). The basal AMPK specific activity with DMSO was taken as 100% (27.07±5.0 μmol/mg of AMPK/min), *$p<0.05$, in comparison with the respective controls.

Figure 4. (**A**) The effect of **34** on the blood glucose level: hyperglycemic KKAy mice were injected s.c. twice daily with sesame oil (150 μl, ■), 34 (30 ▲, or 75 □, mg/kg body weight) for 4 days and blood glucose was measured at the indicated times. The blood glucose levels at day zero, 20.8 ±0.9 and 22.3 ± 1.3 mM for the control and **34** -treated groups, respectively, were taken as the reference 100% values. (**B**) Compound **34** improved glucose tolerance in hyperglycemic KKAy mice: ip-GTT was performed following an overnight fast in mice that had been treated with **34** for 2 days (30 and 75 mg/kg) or oil, as descried under *Experimental section*. Mean ± SEM, n=10 per group for all animal experiments, *$p<0.05$ in comparison with the oil-treated group.

Figure 5. Hydrophobic, aromatic and H-bond acceptor features are represented in blue, orange and green spheres, respectively. (**A**) PT-1 (stick representation) aligned to the pharmacophore model (fit value = 9.00). (**B**) Compound **4** aligned into two, largely non-overlapping parts, of the pharmacophore model (fit values of 2.23 and 2.49 for the left and right parts, respectively). (**C**) Compound **34** aligned to the pharmacophore model (fit value = 4.63).

Figure 6. (**A**) See legend of **Figure 5** for definition of the pharmacophoric features. (**B**) Compound **34** aligned to the pharmacophore model. Pharmacophoric features corresponding to the ethoxybenzothiazole moiety are circled. The H-bond acceptor corresponding to the sulfur atom is marked by an arrow. (**C**) Compound **31** aligned to the pharmacophore model. The mismatch between the NH moiety (H-bond donor) and the H-bond acceptor pharmacophoric feature is marked by an arrow.

Figure 7. (**A**) Binding mode of PT1 within the binding site of AMPK (top). Specific interactions between binding site residues and PT1 moieties are highlighted (bottom). (**B**) Binding mode of compound **34** within the binding site of AMPK (top). Specific interactions between binding site residues and **34** moieties are presented (bottom).

Scheme 1. (a) NaH, alkylhalide, dry THF, 0 °C to rt, approximately 2 h. (b) *n*-propylamine, HOBt, EDC, $CHCl_3$, rt, overnight. (c) $AlCl_3$, $(CH_2Cl_2)_2$, rt, overnight. (d) 28% NH_4OH, 5.25% NaOCl, 6% NaOH, 0 °C, 15 min. (e) 6% $KMnO_4$, Me_2CO, rt, 1.5 h.

Scheme 2. (f) concentrated HCl, THF, reflux, overnight.

Scheme 3. (g) trichloroisocyanuric acid, $CHCl_3$, reflux, overnight. (h) commercially available amine or **4**, triethylamine, DMAP, THF, rt or reflux, overnight.

Table of Contents Graphic

TOC Abstract